12-2005

An Experimental Evaluation of the Constant β Relating the Contact Stiffness to the Contact Area in Nanoindentation

Jeremy Harper Strader
University of Tennessee - Knoxville

To the Graduate Council:

I am submitting herewith a thesis written by Jeremy Harper Strader entitled "An Experimental Evaluation of the Constant β Relating the Contact Stiffness to the Contact Area in Nanoindentation." I have examined the final electronic copy of this thesis for form and content and recommend that it be accepted in partial fulfillment of the requirements for the degree of Master of Science, with a major in Materials Science and Engineering.

George Pharr, Major Professor

We have read this thesis and recommend its acceptance:

Warren Oliver, T. G. Nieh

Accepted for the Council:
Carolyn R. Hodges

Vice Provost and Dean of the Graduate School

(Original signatures are on file with official student records.)

To the Graduate Council:

I am submitting herewith a thesis written by Jeremy Harper Strader entitled "An Experimental Evaluation of the Constant β Relating the Contact Stiffness to the Contact Area in Nanoindentation." I have examined the final electronic copy of this thesis for form and content and recommend that it be accepted in partial fulfillment of the requirements for the degree of Master of Science, with a major in Materials Science and Engineering.

George Pharr
Major Professor

We have read this thesis
And recommend its acceptance:

Warren Oliver

T. G. Nieh

Accepted for the Council:

Anne Mayhew
Vice Chancellor and
Dean of Graduate Studies

(Original signatures are on file with official student records).

An Experimental Evaluation of the Constant β Relating the Contact Stiffness to the Contact Area in Nanoindentation

A Thesis

Presented for the

Master of Science

Degree

The University of Tennessee, Knoxville

Jeremy Harper Strader

December, 2005

Dedication

This thesis is dedicated to Dionysus the god of celebration and the divine extraction of libation from the vined fruit for which your praises will be sung on high upon the completion of this thesis.

Acknowledgments

This research was sponsored by the Division of Materials Science and Engineering, Office of Basic Energy Sciences, U.S. Department of Energy, and the SHaRE Collaborative Research Center at Oak Ridge National Laboratory, under contract DE-AC05-00OR22725 with UT-Battelle, LLC.

Abstract

Measurements of mechanical properties by nanoindentation with triangular pyramidal indenters like the Berkovich rely heavily upon the relationship between the contact stiffness, S, the contact area, A, and the reduced elastic modulus, E_r . This relationship is often written in the form: $S = 2\beta E_r(A/\pi)^{1/2}$, where β is a constant that depends on the geometry of the indenter. Although the most common values for β used in experimental measurements are 1.000 and 1.034, various theoretical analyses have yielded values as small as 1.00 or as large as 1.2, depending on the assumptions made to model the deformation. Here the most appropriate value of β is explored by performing careful experiments in fused quartz with thin gold coatings applied to the surface to reveal the actual contact area when observed in the scanning electron microscope. Experiments were performed not only with the Berkovich indenter, but with five other three-sided pyramidal indenters with centerline-to-face angles ranging from 35.35^o (cube corner) to 85^o. Results are discussed as they apply to using the correct value of β in order to correctly determine indenter area functions and obtaining accurate measurements of mechanical properties.

Table of Contents

List of Tables

List of Figures

1 Introduction

The measurement of mechanical properties by nanoindentation relies heavily on the well-known relation between the contact stiffness, S, the contact area, A, and the reduced elastic modulus, E_r:

$$S = 2\beta E_r \sqrt{\frac{A}{\pi}} \qquad 1$$

where

$$\frac{1}{E_r} = \frac{1-\nu_s^2}{E_s} + \frac{1-\nu_i^2}{E_i}, \qquad 2$$

and β is a constant that depends primarily on the geometry of the indenter[1],[2],. In Eq. 2, E is Young's modulus and ν is Poisson's ratio, and the subscripts s and i designate the specimen and indenter, respectively. In using Eq. 1 to make property measurements, the contact stiffness S is usually a measured parameter, and quantities such as E_r and A are derived from it by means of Eq 1. However, to do so requires an accurate value for the geometric constant β. For the Berkovich triangular pyramidal indenter frequently used in nanoindentation work, numerous values for β ranging from 1.00 to 1.20 have been suggested based on theoretical considerations, but no single value stands out as preferred [3]. In practice, the value $\beta = 1.034$ is often used, but this is based on an analysis that models elastic contact by a flat triangular punch which ignores the true 3-dimensional nature of the Berkovich pyramid [4].

Error in the value used for β affects the results calculated from nanoindentation studies. Most notably, if the value of β used is off by 2%, assuming the indenter's projected area is known, then the reduced modulus calculated will be off by 2% and the hardness calculated will be off by a little more than 4%. If the stiffness equation is used with an incorrect value for β to do a tip calibration such on a material of known E_r as outlined in Hay [5], then the resultant area function determined is off by approximately twice the error in β by virtue of the stiffness equation. If this incorrect area function is used in an attempt to determine E_r for another material, the β's cancel:

$$E_{r2} = \frac{\beta S_2 E_{r1}}{\beta S_1}, \tag{3}$$

and the correct value is found; however, if this area function is used to calculate the hardness of the new material:

$$H = \frac{P_2}{A} = \frac{P_2}{4\pi\left(\frac{S_1}{\beta E_{r1}}\right)^2}, \tag{4}$$

where β fails to cancel yielding approximately twice the error in the measured hardness as is in β.

The goal of this study was to measure the value of β is in a commonly used calibration material fused quartz, as well as, its relationship to the indenter's centerline-to-face angle α. To this effect, six different pyramidal indenters with varying centerline-to-face angles α (see Figure 1) are used. To this effect, best possible measurements of the variables in the stiffness equation were made in order to arrive at a value for β.

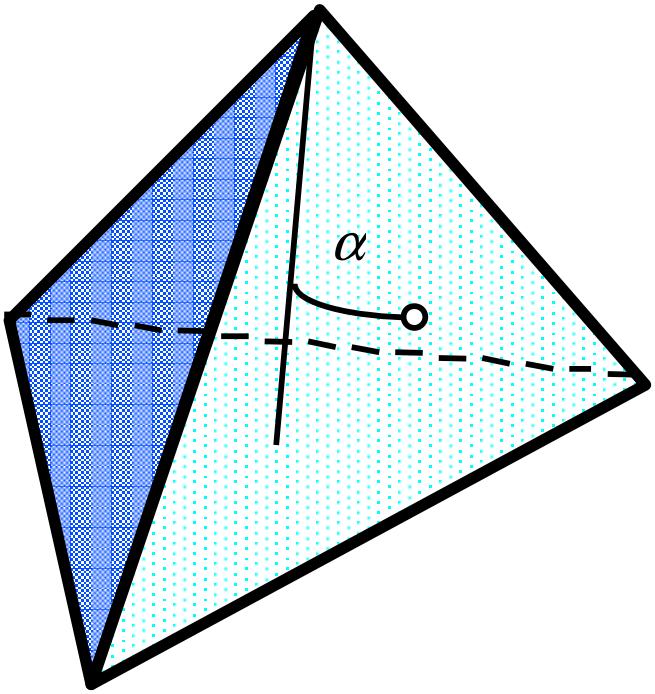

Figure 1 Three-sided pyramidal indenter

The indenters used in this study are listed in Table 1 with their equivalent cone angles ψ (shown in Figure 2), which provides the same depth-to-area ratio as the pyramids of angle α. The tips used were new, and should not exhibit tip rounding beyond the initial manufacturing defect.

Table 1 Summary of indenters used in this study

Centerline-to-face α degrees	Equivalent Cone Angle ψ degrees	Area (projected) A(h)
35.26 (Cube-Corner)	42.28	$2.60h^2$
45	52.13	$5.20h^2$
55	61.43	$10.60h^2$
65.3 (Berkovich)	70.32	$24.56h^2$
75	78.23	$72.37h^2$
85	86.11	$678.86h^2$

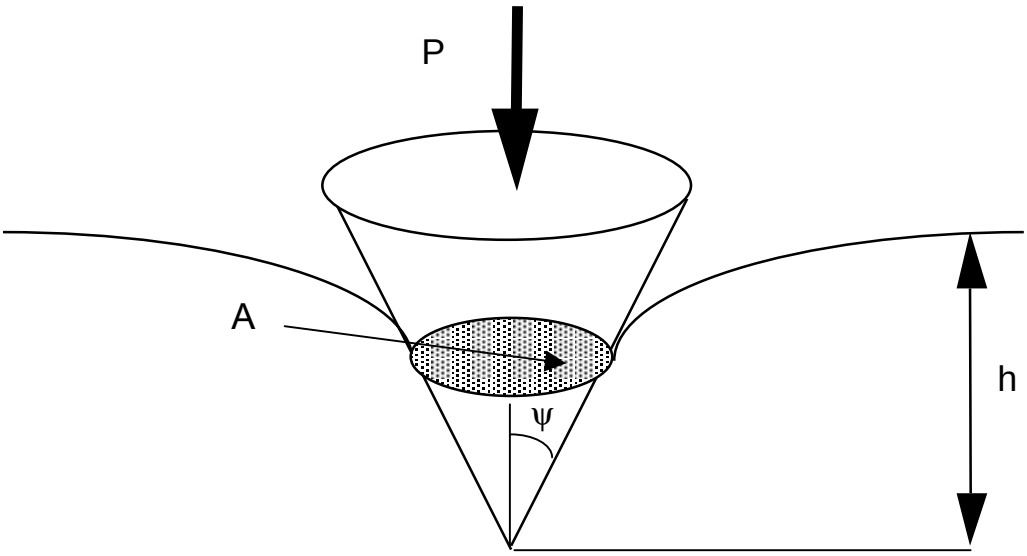

Figure 2 Schematic of indentation with a cone

2 Experimental Procedures

2.1 Sample Preparation

Polished specimens of Fused Quartz were obtained from MTS Nano Instruments. Three specimens were used in this work which will be referred to as Samples A, B, and C. All samples were masked with card stock to protect a portion of the surface during the gold coating process leaving them unaltered. Sample A was then placed into the gold coating machine pictured in Figure 3, and an 11 nm coating was applied by sputtering. This coating was applied in such a way that caused the coating to develop very small cracks, which when contacted by an indenter, smooth out providing excellent contrast between areas that were in contact and those that were not. Samples B and C were coated with a uniform 5nm thick coating. The thickness of the coating was determined by the change in resonance frequency of a quartz crystal.

2.2 Sample Leveling

Small misalignments of the sample surface relative to the direction of motion of the indenter can produce significant asymmetries in the contact geometry [3]. To avoid this, a special specimen mount was used in conjunction with an interference microscope to level the samples to within 0.1^{o}. To this end, a selenium sample was permantly placed into the sample tray. Selenium samples by nature have a very smooth and slightly rounded surface. It was then indented over fifty times covering the entire sample. The indents

Figure 3 SPI gold coating machine

were then observed, and the indent that was the most equilateral was marked as shown in Figure 4. Assuming that the indenter is perfectly aligned with respect to its direction of motion, the calculated error in area calculation due to sample tilt was less than %0.004. Using an ADE Phase Shift MicroXam® interference microscope (Figure 6), the stage was leveled to make the material surrounding the indent as level as possible Figure 5. In place of a standard cylindrical sample holder, a special one was constructed (see Figure 7) that allows set screws to finely adjust the tilt of the sample itself. This special sample holder also employs conical washers at the base of the large screw to allow it to be tightened enough to ensure that the sample holder is sufficiently stiff, so that it does not affect the stiffness measurement. A representative Berkovich indent that was leveled using this method is shown in Figure 8. Sample and indenter misalignments alter the geometry of the problem causing larger contact areas for a specified depth than would be attained with a perfectly aligned indenter and sample making the measured hardness and stiffness higher.

Due to the inherent complexity of the geometrical problem of misalignment, the importance of misalignment was examined numerically using a program written in MATLAB® that calculates the sample misalignment and overestimation in the projected area and the indenter misalignment with respect to its direction of travel from only the lengths of the three sides of a residual hardness impression, assuming a perfect pyramidal indenter. The three side measurements are shown in Figure 9. The concept of this program was based on a graphical solution presented in [6]. Using this program, the overestimation of the projected area for a typical indent shown in Figure 8 was calculated

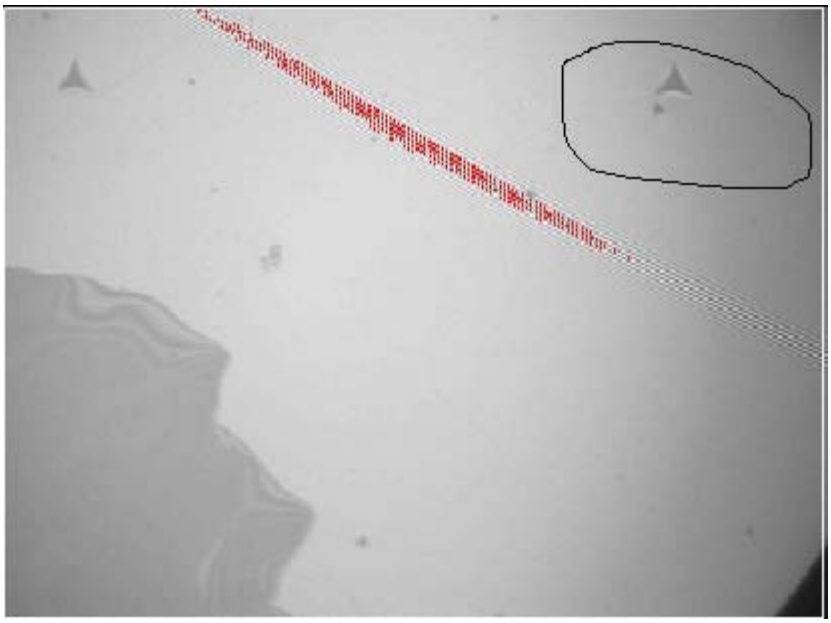

Figure 4 Near perfect indent in selenium

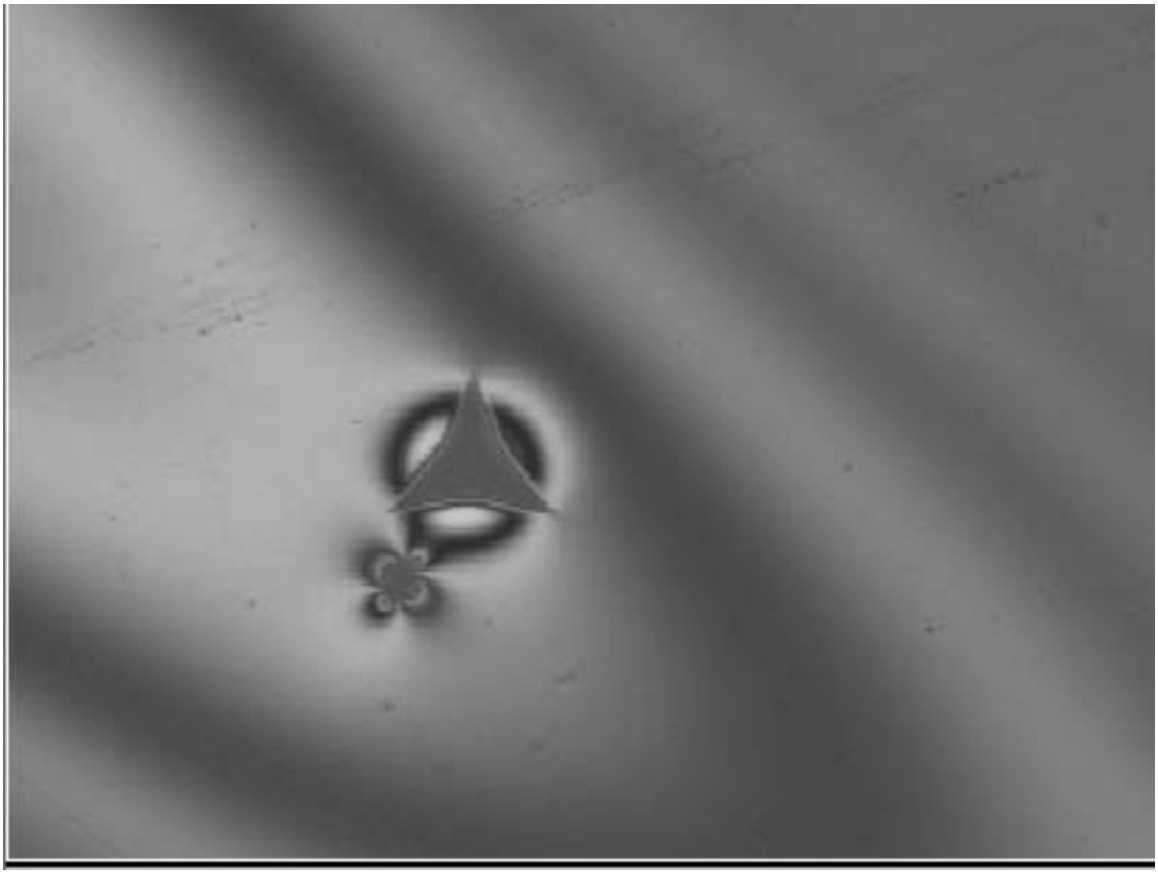

Figure 5 Selenium sample leveled in the MicroXam to near perfect indent.

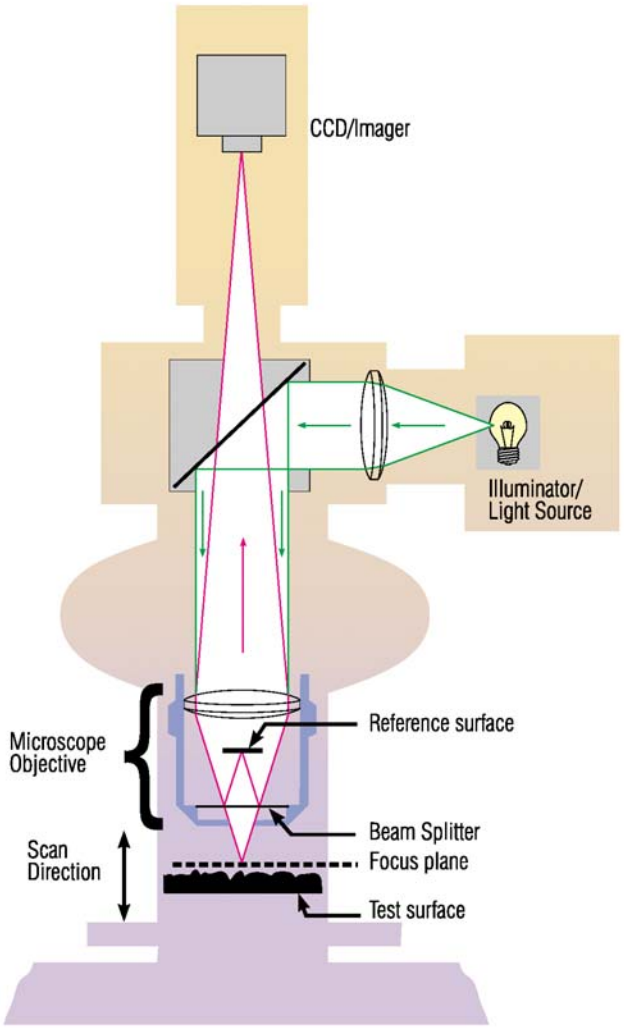

Figure 6 MicroXAM® interference microscope

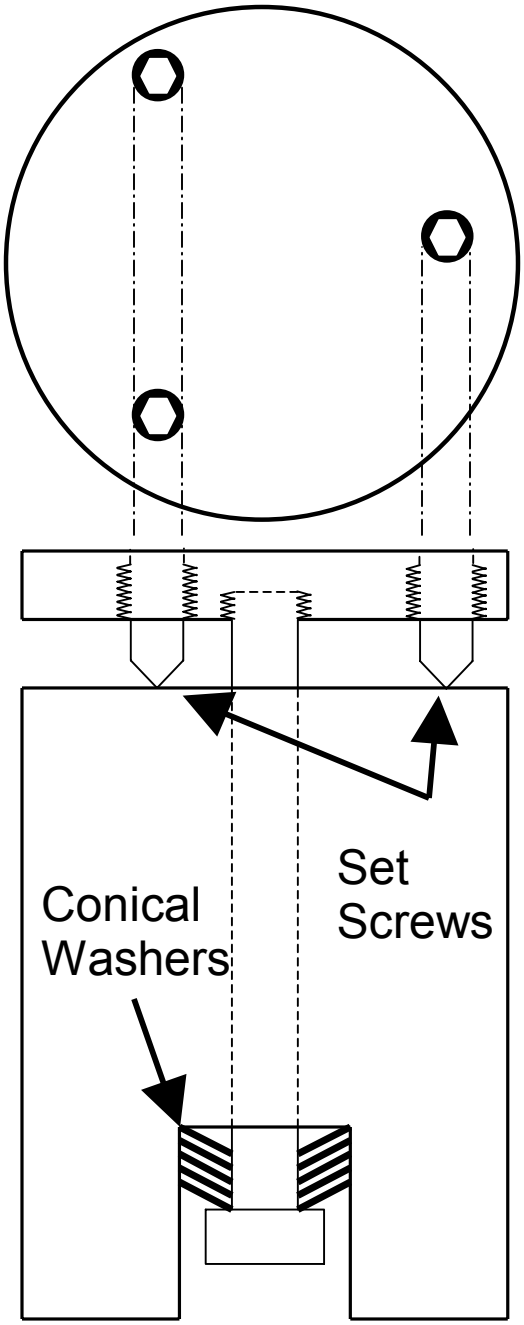

Figure 7 Sample leveling device

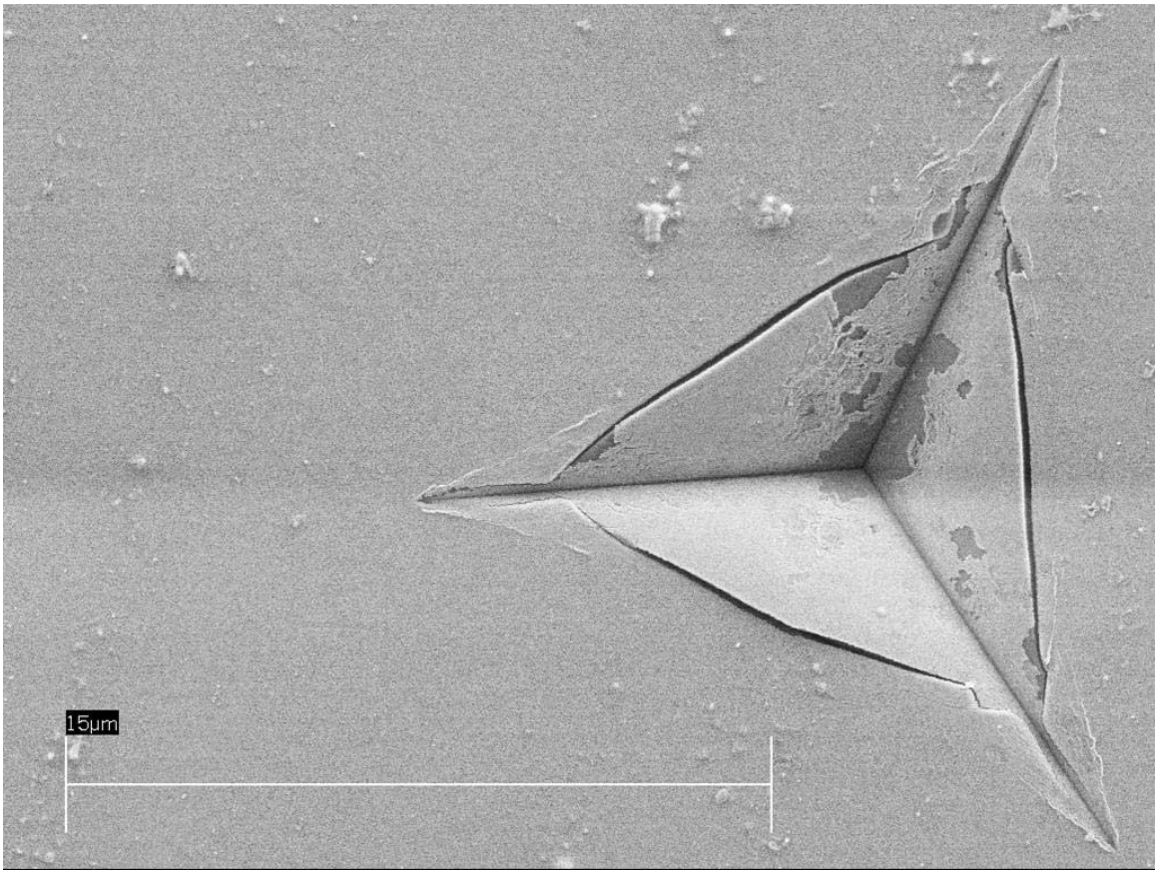

Figure 8 Leveled Berkovich indent in fused quartz

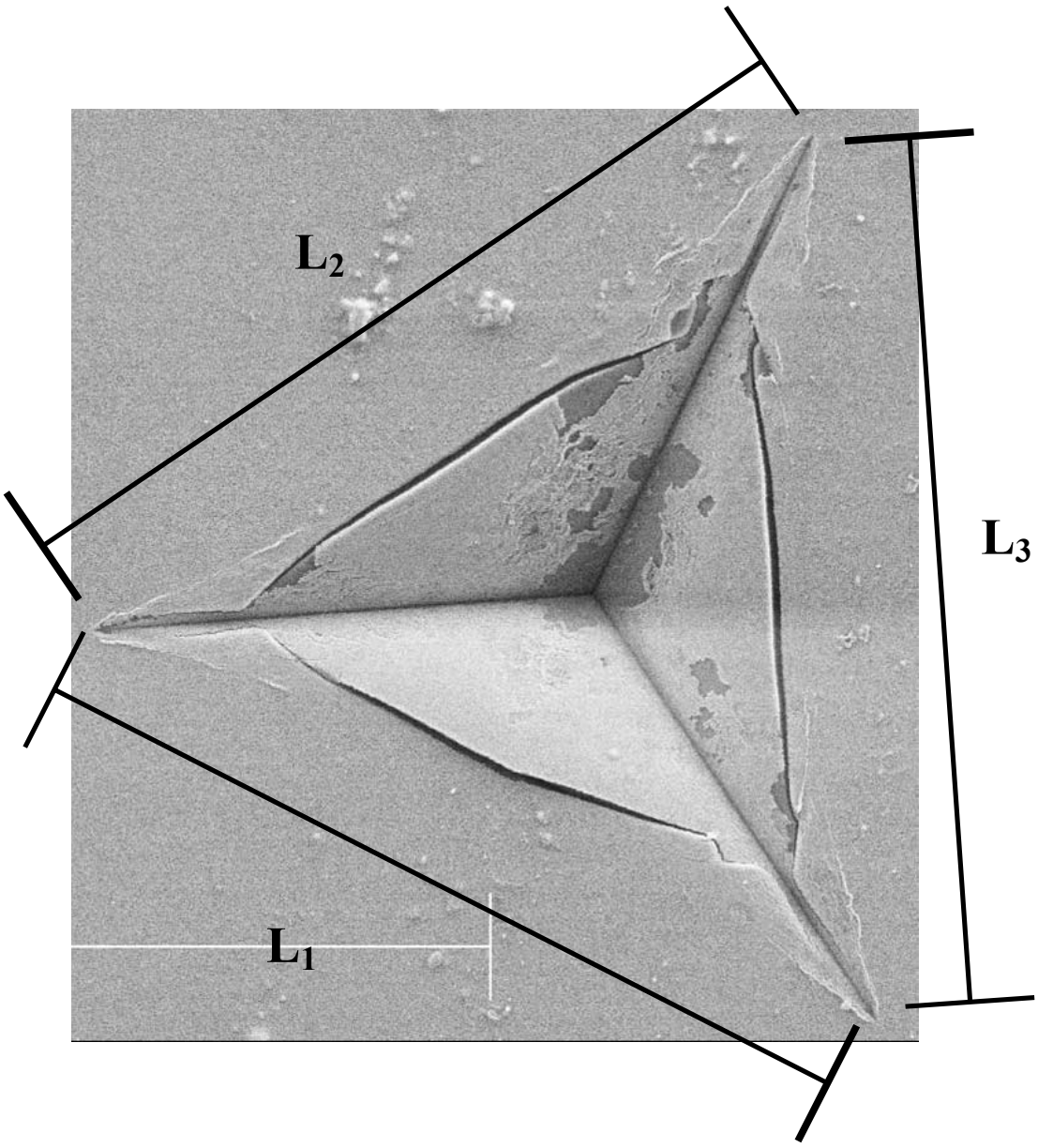

Figure 9 Measuring the three side lengths

to be %0.04 assuming perfect indenter alignment with respect to its direction of travel. The assumption of a perfectly aligned indenter was assumed reasonable due to the very small error associated with small misalignments. The effect of misalignment of the sample and that of the indenter is shown in terms of the shortest (l_1) and longest (l_3) measured sides of the indent (right axis) and misalignment of indenter (left axis), with Figure 10 showing the minimum increase of contact area and Figure 11 showing the maximum. The difference between the two graphs is caused by the length of the intermediate side.

2.3 Nanoindentation

Indentations were made in fused quartz specimens with a Nanoindenter XP® (MTS Systems Corp, Knoxville, TN) operated in the continuous stiffness measurement mode, shown schematically in Figure 12 and pictured in Figure 13. In order to reduce test time, and minimize errors due to thermal drift, upon surface detection by the nanoindenter, a constant loading rate is applied for a few seconds until the indenter penetrates 50nm into the sample. Then, the load was increased according to:

$$\frac{\dot{P}}{P} = 0.05 s^{-1}, \tag{5}$$

which maintains a constant indentation strain rate. The indentation rate is given by:

$$\frac{\dot{h}}{h} \tag{6}$$

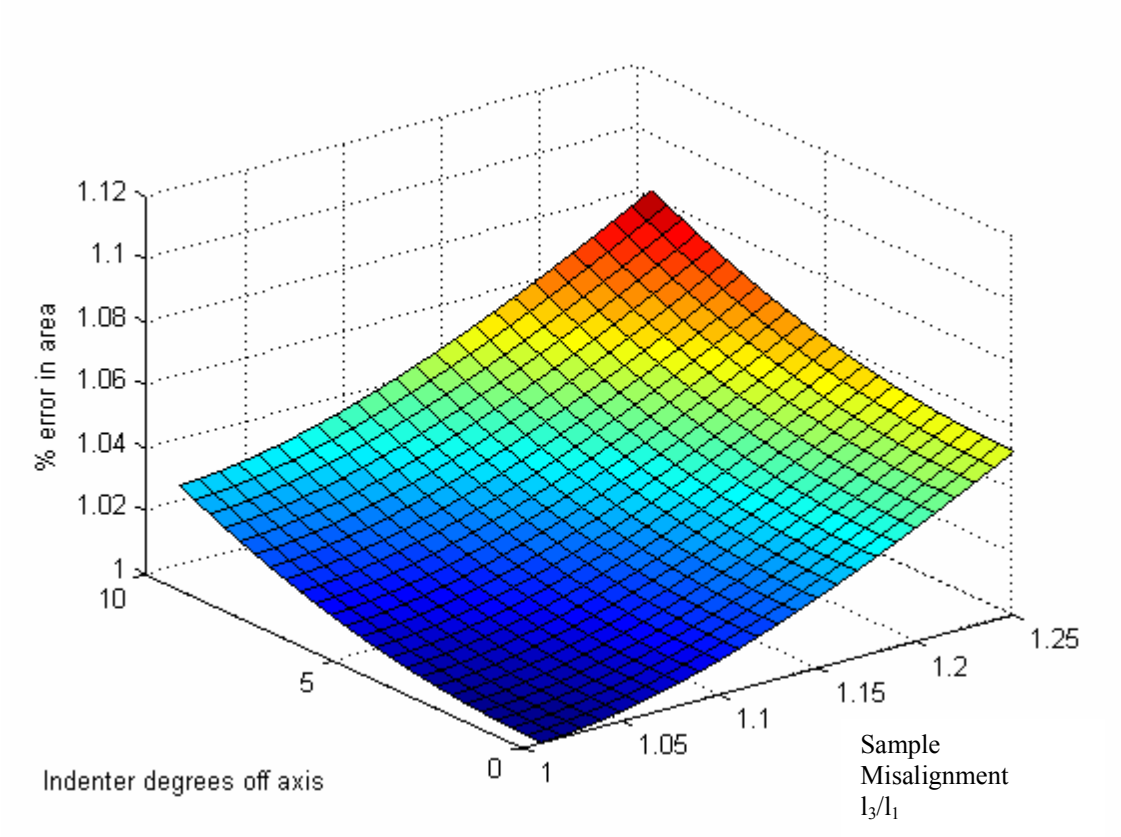

Figure 10 Minimum error vs. side lengths, and indenter misalignment (long intermediate side)

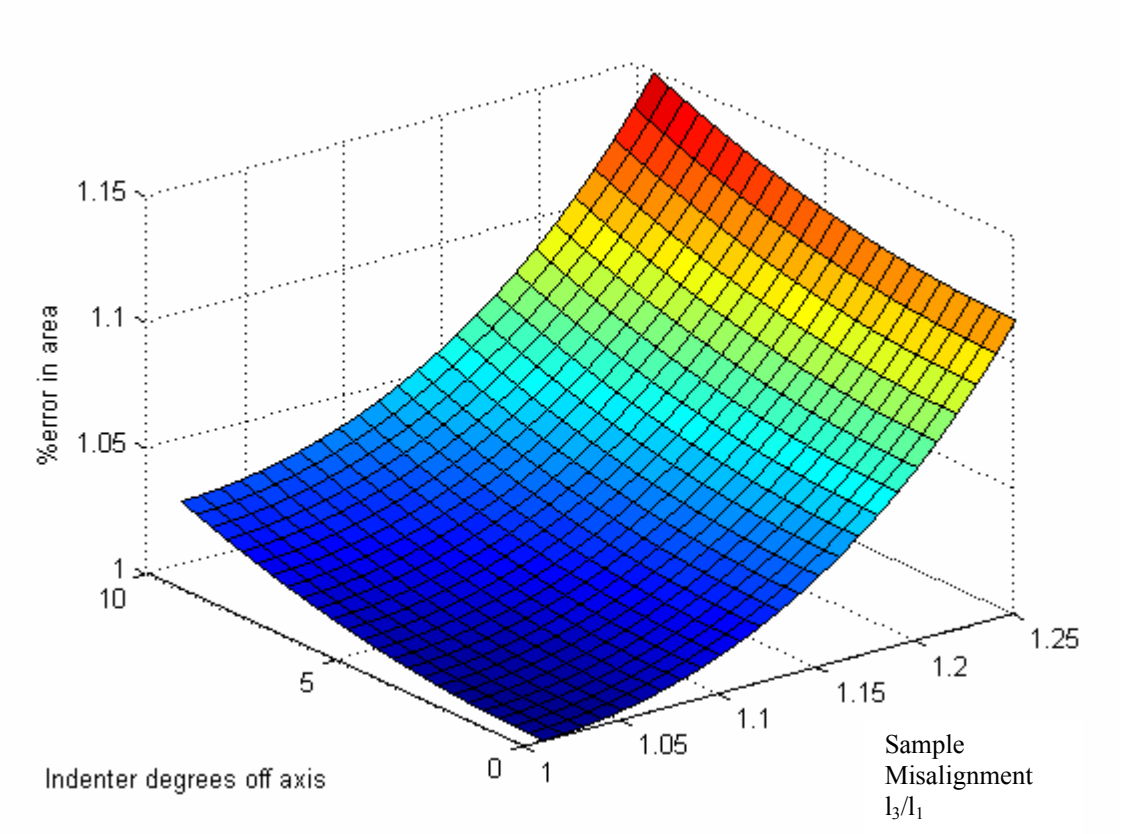

Figure 11 Maximum error vs. side lengths, and indenter misalignment (short intermediate side)

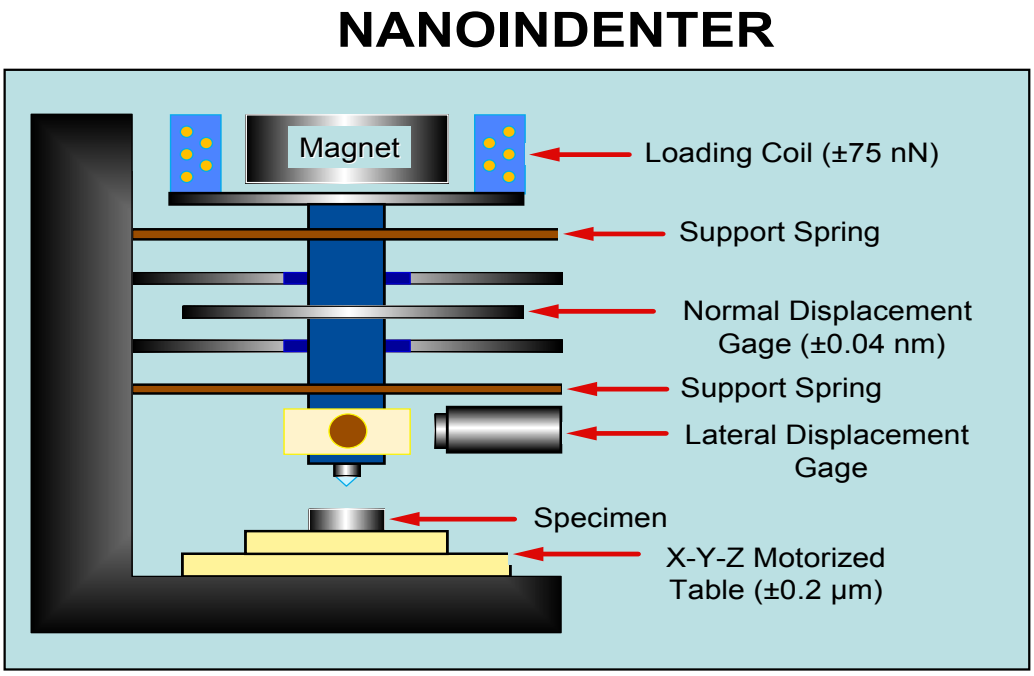

Figure 12 Nanoindenter schematic

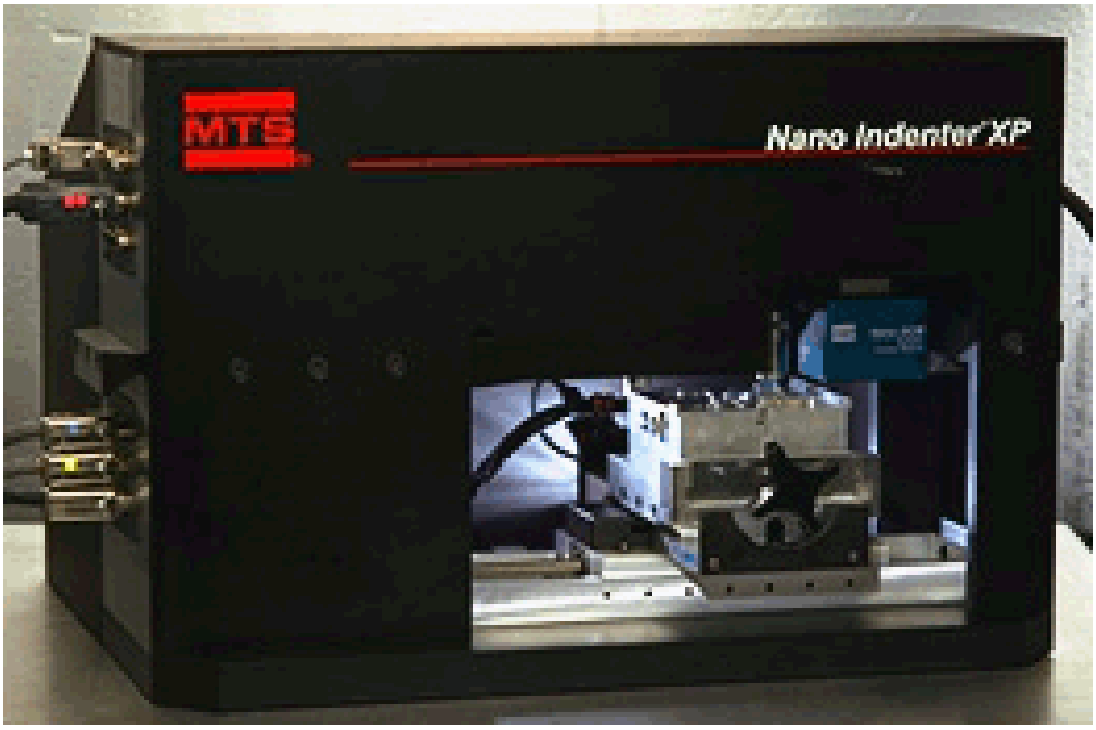

Figure 13 MTS®Nano Indenter XP

where h is the indenter dept of penetration and $\dot{h}$ is the rate of penetration. In the case of the α = 65°, 75°, and 85° degree indenters, the loading phase ended when the harmonic load exceeded 5200 μN. This value was chosen because it is just below the machine maximum of 5500μN. For the cases of the sharper indenters, the maximum load was chosen just below the cracking threshold, except for the 35^o indenter for which it was unavoidable. The maximum load and displacements are shown in Table 2. The harmonic displacement for all tests was chosen to be 7nm, as it allowed us to penetrate to maximum depths while minimizing scatter in the stiffness measurement. The maximum load was then held for 10 seconds to let the harmonic oscillation stabilize without causing significant creep, and then unloading began.

2.4 Elastic Property Measurement

The elastic properties normally assumed for fused quartz are E_s = 72.0 GPa and ν_s = 0.17, and for diamond E_i = 1141 GPa and ν_s = 0.07 [1], giving a reduced modulus of E_r = 69.6 GPa. To assure accurate measurements for the fused quartz used in this study, Dr. Hongin Bei measured its elastic constants to 3 digit accuracy using standard ultrasonic techniques [7]. The density needed to compute the elastic constants from the ultrasonic wave velocities was measured by pycnometry to be 2.253 g/cm^3. The values of E and ν so determined were 73.1±0.4 GPa and 0.13±0.01, respectively, giving E_r = 69.8±0.4 GPa [7].

Table 2 Indentation parameters

Centerline-to-face α (degrees)	Sample	# of Tests	Maximum Load P (mN)	Maximum Depth h (nm)
35.3 (cube corner)	C	3	80	2000
45	B	3	120	1760
55	A	4	420	2640
65.3 (Berkovich)	A	7	730 approx.	2700
75	A	5	730 approx.	2000
85	A	3	310 approx.	650

2.5 Stiffness Measurement

Classically, the stiffness is calculated by modeling the unloading curve using the power law relation:

$$P = \alpha \left(h - h_f \right)^m \qquad 7$$

where h_f is the residual depth of the indent, and α and m are fitting constants. The stiffness is then evaluated by taking derivative of this this equation with respect to h at maximum depth [6]. An alternative method to determine the stiffness is known as the continuous stiffness method (CSM). Stiffness is measured throughout the test by applying a sinusoidal oscillation to the applied force and measuring its effect on displacement. This method proved beneficial for this work because it exhibited less scatter and required no estimation of residual depth h_f.

In order to avoid complications arising from the gold film, the stiffnesses were also measured in an adjacent uncoated area on the same fused quartz specimen and compared to those measured in the coated areas. All tests were conducted using a relatively large harmonic displacement of 7nm to achieve the desired accuracy and a 10 second hold at maximum load during which the stiffnesses were determined. The value chosen for the stiffness was the average of the stiffnesses collected at the end of the hold period when the noise had settled down to an acceptable level. A representative harmonic stiffness measurement is shown in Figure 14 for a 75^o indenter. The measured stiffnesses typically exhibited less than 1% scatter.

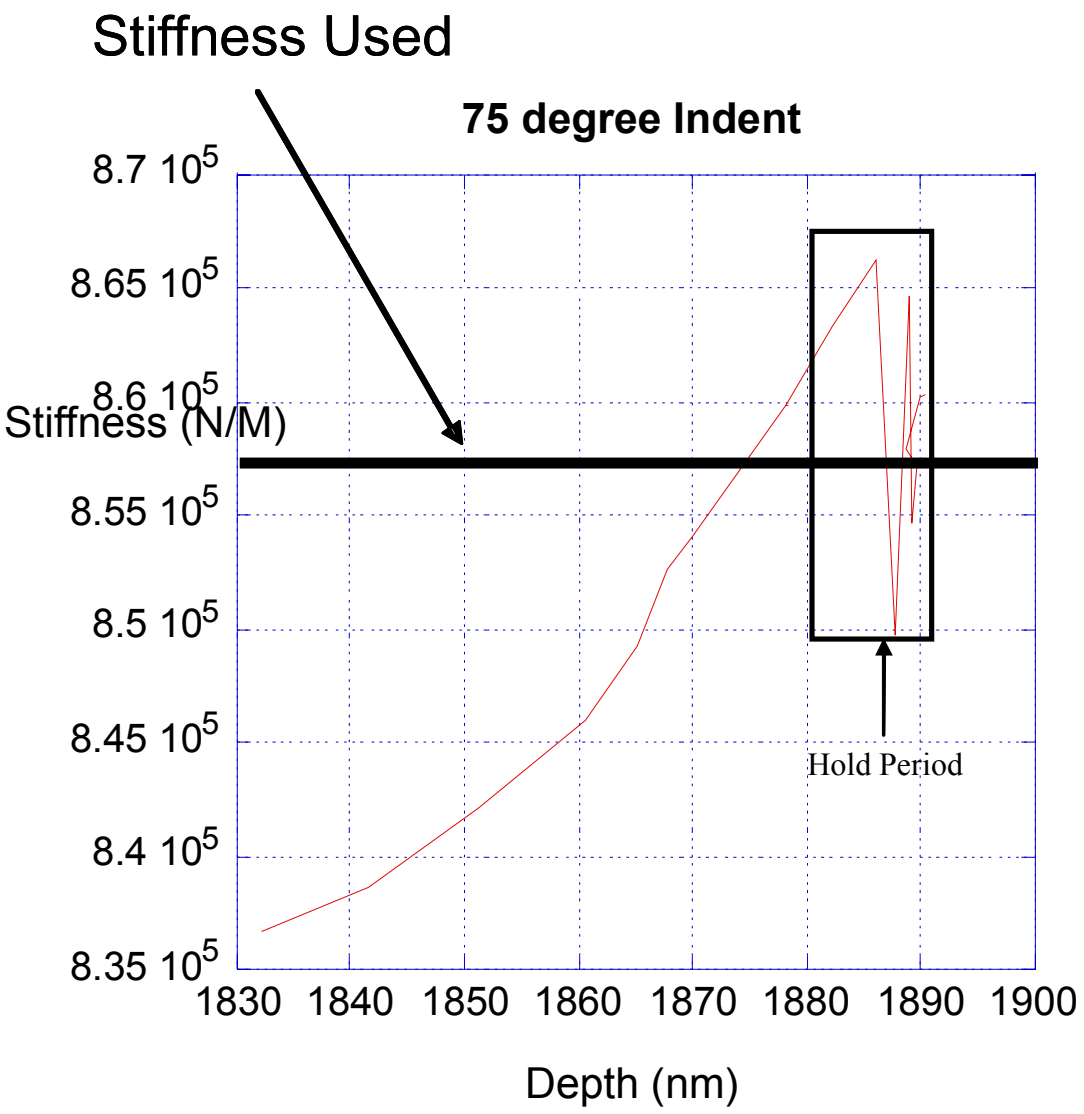

Figure 14 Choice of stiffness value for a typical indent during the hold period

The load frame compliance C_m is the measure of the compliance of the machine, while C_t is the total compliance measured. The stiffness and depth of penetration must be corrected to take this into account using

$$C_t = \frac{1}{S} + C_m \qquad 8$$

and

$$h = h_t - C_m P \qquad 9$$

where h is the depth of penetration of the indenter into the sample and h_t is the total displacement of the indenter.[2]. C_m was determined using the assumption of constant hardness for which:

$$\frac{P}{S^2} = k \qquad 10$$

is satisfied for large depths of penetration [6]. This load frame compliance was verified for two different Berkovich indenters in several different fused quartz samples. The maximum error in the measured stiffness due to the choice of load frame compliance was estimated at 0.5%.

2.6 Area Measurement

Contact areas were measured from SEM micrographs with magnifications verified by imaging 1.07±0.01 μm diameter latex calibration spheres (Figure 15), at several different SEM conditions that were representative of those used in this study. As shown in Figure 16, it is extremely difficult to identify the true edges of contact from normal SEM or optical images of indentations in fused quartz. There is not an abrupt

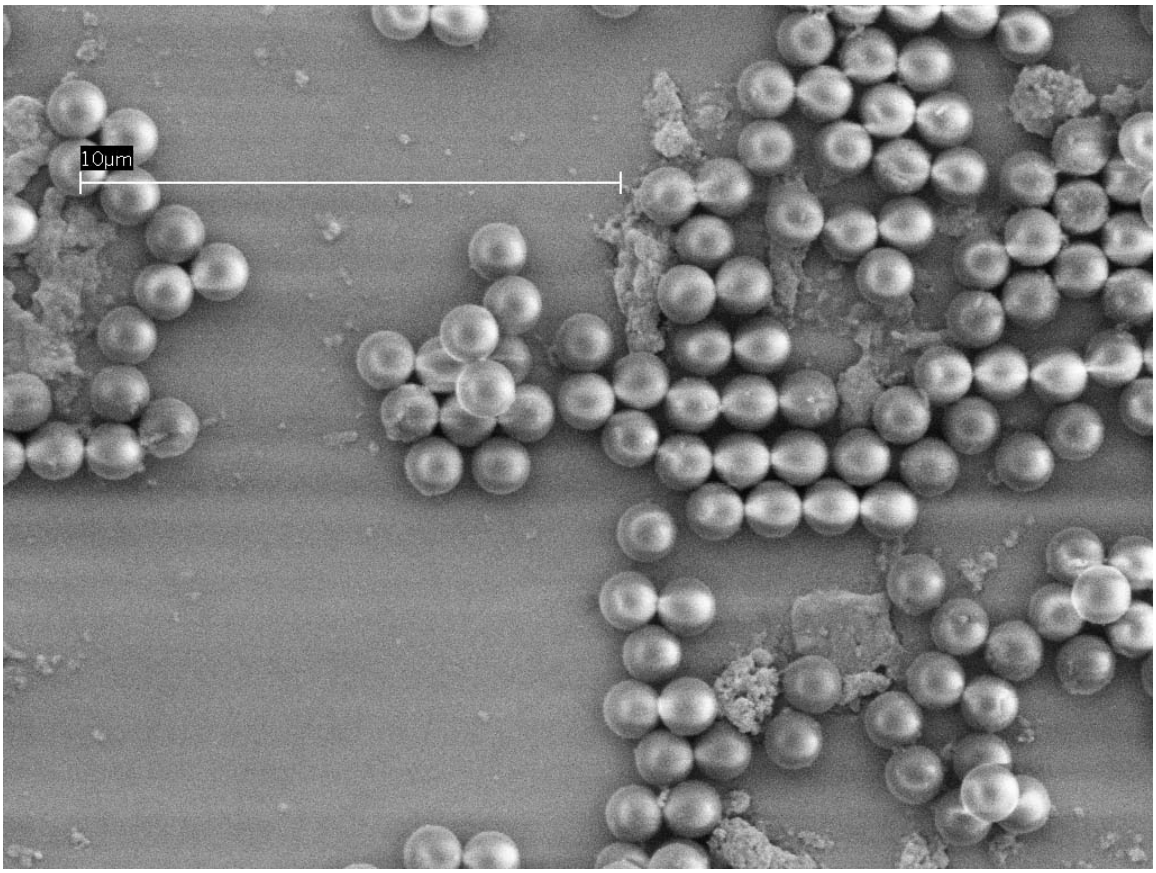

Figure 15 SEM image of 1.07µm calibration spheres at a typical magnification used

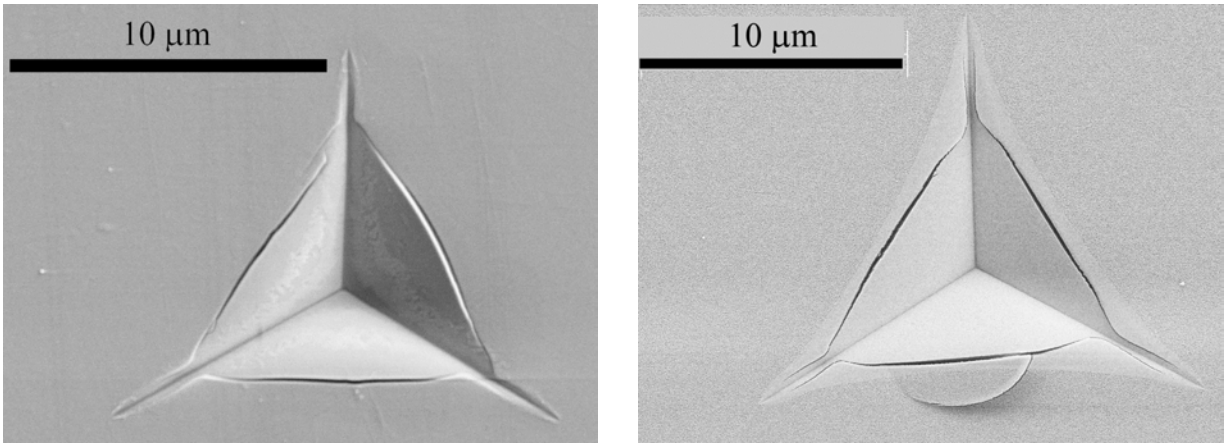

(a) **(b)**

Figure 16 Berkovich indentation in fused quartz: (a) uncoated; (b) gold coated

change in the surface profile at the contact edge, and cracks that form near the perimeter of the contact can be misconstrued for the contact edge itself (Figure 16a). To circumvent this problem, specimens were first coated with thin gold coatings 5 and 11 nm thick and then indented. As shown in Figure 16b, plastic deformation in the film clearly delineates the contact perimeter. It is evident that the contact area at peak load extends well beyond the cracks. For the indent shown in Figure 17, the actual contact area (red) was 86.9 μm^2; in contrast, the area estimated from the cracked edges (green) was 58.2 μm^2 and the area determined from the corners of the contact assuming a perfect triangle (blue) was 121 μm^2.

A representative 75^o indent was also measured using an interference microscope for comparison to the SEM. A comparison of the two areas measured is shown in Figure 18. The tips of the edges line up almost perfectly, but the determination of the contact edge on the face show the drawbacks of this method. The actual points of contact on the interference micrograph are arbitrary (save the tips of the edges), and depend on what amount of surface deformation the user chooses to define contact.

Measurements for the large angle indenters were conducted on sample A which had a cracked gold coating of 11nm thickness. The contact edge for these indenters was taken as the boundary between the cracked and the partially smoothed gold film in the SEM images. For the large angle indenters especially near the corners there is a region where the gold coating only shows partial deformation (Figure 19). Indents were examined in this region from samples that had gold coatings of varying thicknesses ranging from 2nm to 11nm. The change in shape of the apparent contact edge with

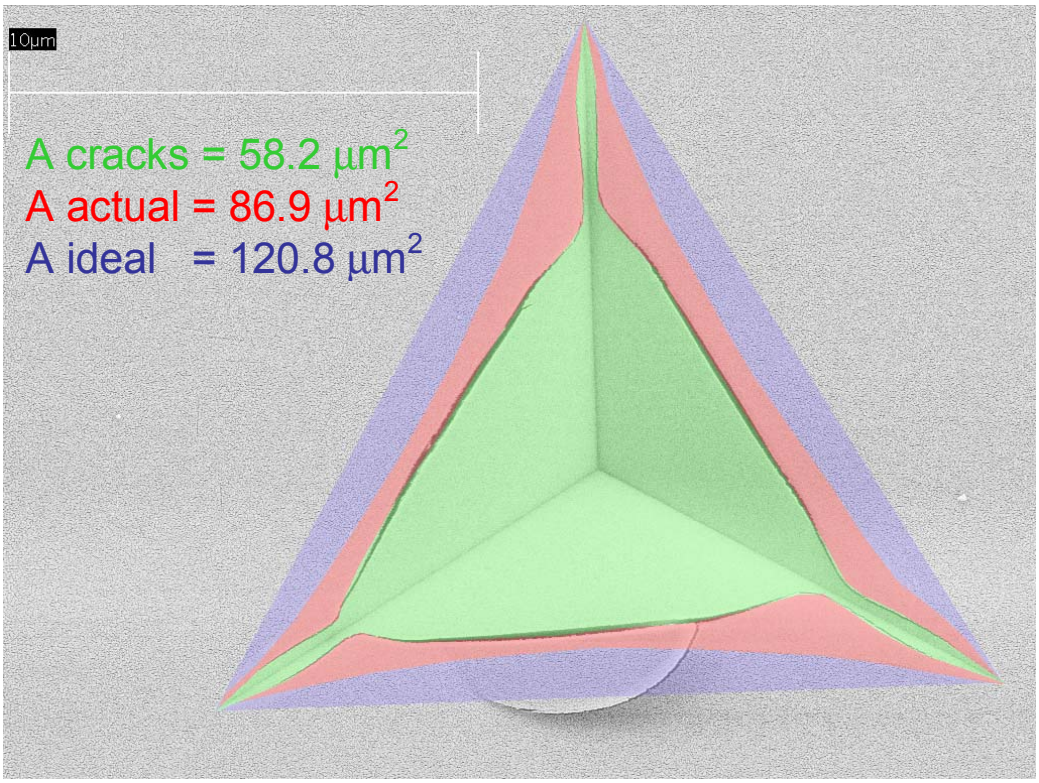

Figure 17 Three different methods of determining contact area

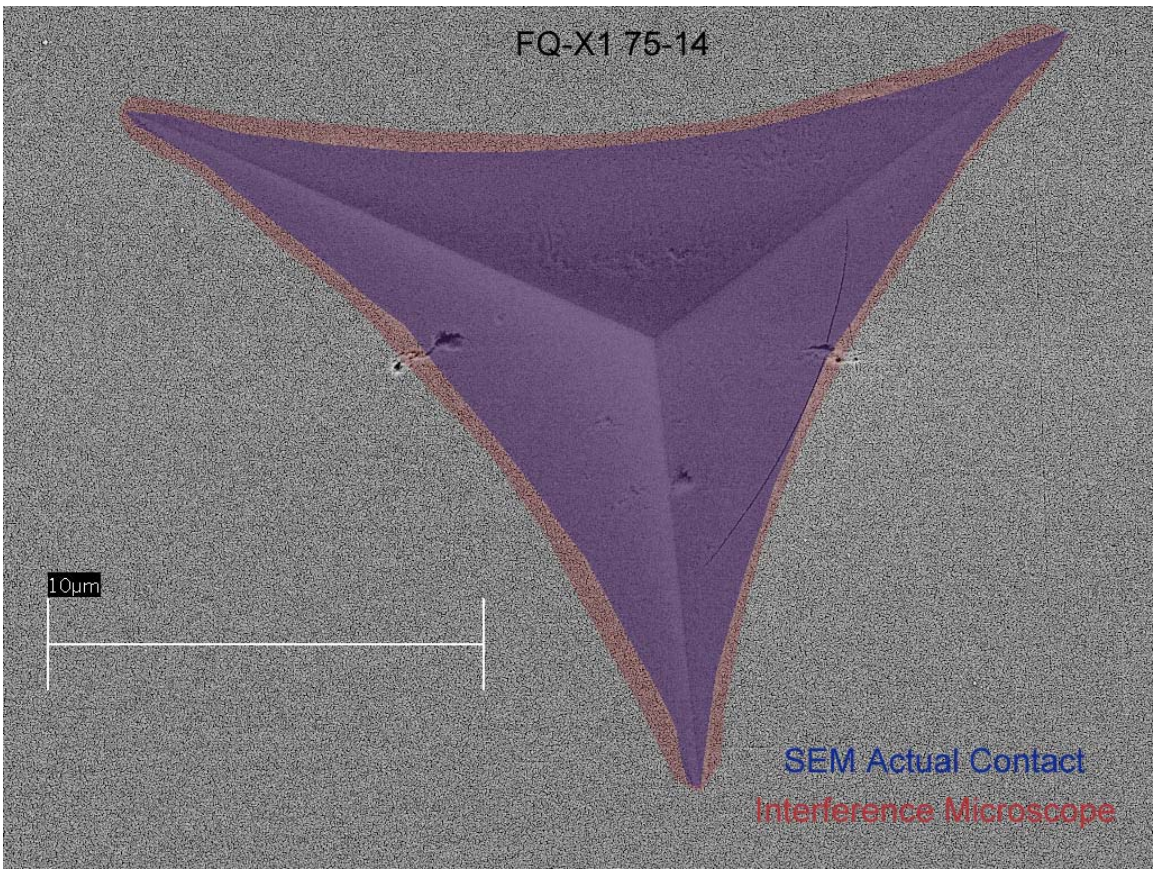

Figure 18 75 degree indent, interference microscope vs. SEM

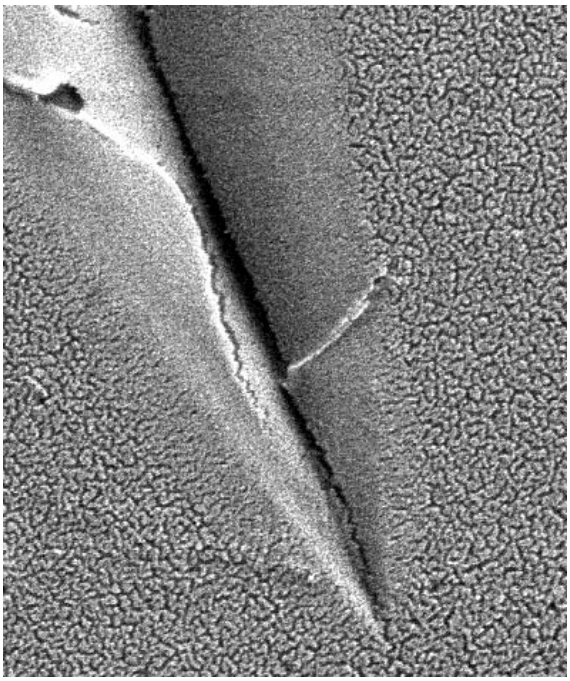

Figure 19 Corner of a Berkovich indent on a sample with a 4nm coating showing partial contact with gold coating

respect to film thickness was negligible. A representative indent is shown in Figure 20 with the choice of its contact area shown in Figure 21. The choice of exactly where to define the edge of contact for these indenters due to partial smoothing of the gold cracks has little effect on the contact area measurement for all wide angle indenters save the 85°.

The smaller angle indenters (35° and 45°) showed significant extrusion of the gold coating at the edge of contact with the indenter, making contact area determinations using the flattening of the cracked surface of the gold coating impossible. In these cases a 5nm gold coating was used to keep the volume of extruded material low while remaining thick enough to minimize image distortion due to charging. The edge of contact was taken to be the inside edge of the extruded gold material (white area in Figure 22). Some of this material was removed by the indenter upon unloading. These areas appear as the darker regions between the extruded gold in Figure 22. The choice of contact area is shown by the colored region in Figure 23.

The $\alpha = 55^{o}$ indenter was too blunt to extrude the gold material out for the 5nm samples making it impossible to determine the contact area using that method, and it exhibited some extrusion on the 11nm sample which adds . On the 11nm sample, determination of the contact edge for this indenter was made using a combination of the disrupted cracks when no extrusion was present, and the inside of the extruded material for areas that had extruded. This effect is shown in Figure 24 with its choice of contact area shown in Figure 25. Only the few indents where the contact edge was relatively easy to identify were used in this study.

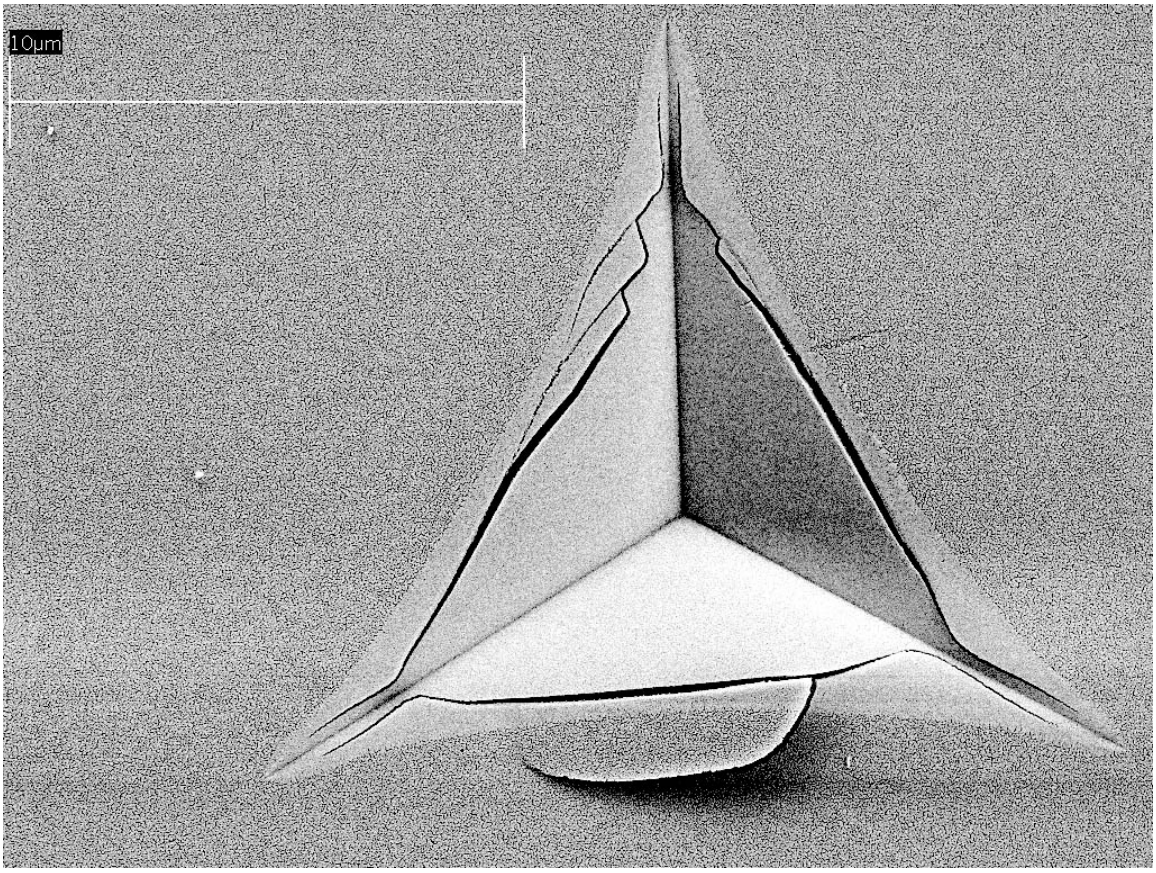

Figure 20 Berkovich indent in gold coated fused quartz, P_{max} = 730mN

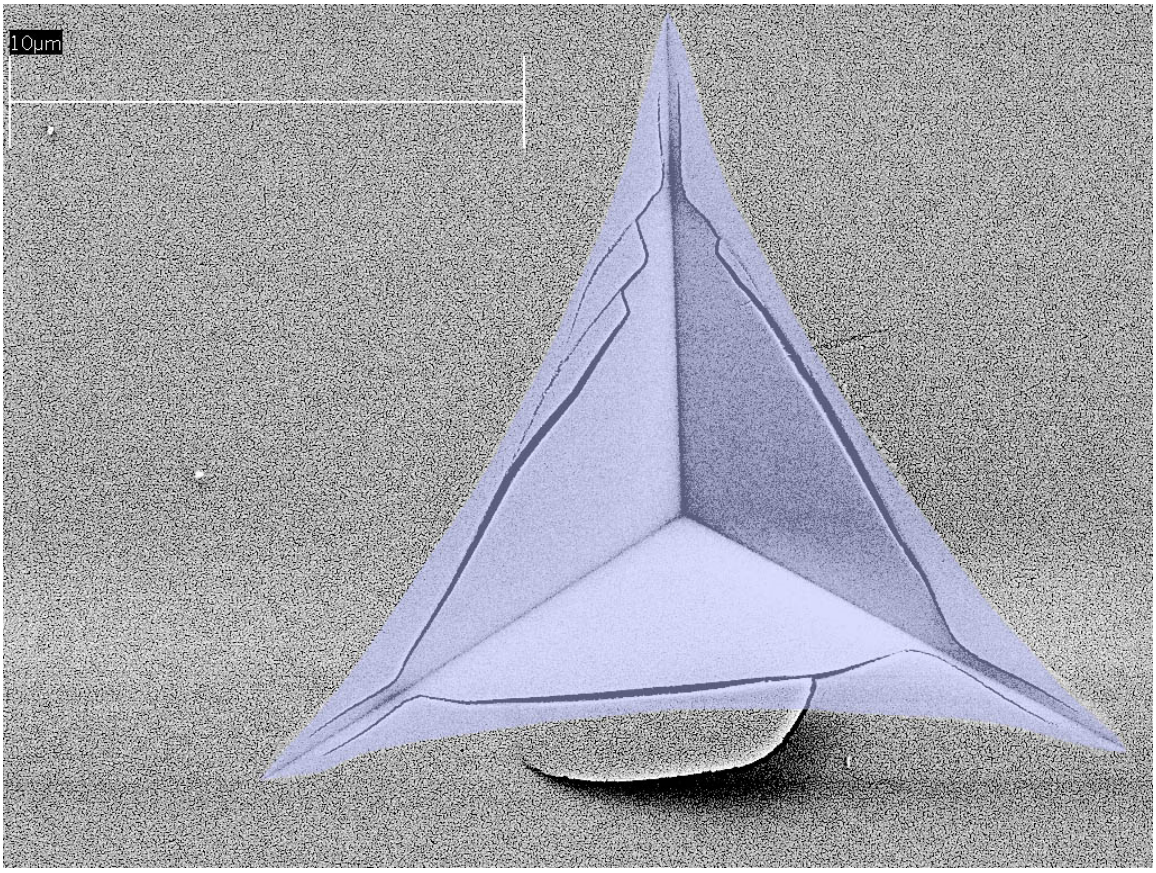

Figure 21 Berkovich indent with colored region showing choice for contact area, P_{max} = 730mN

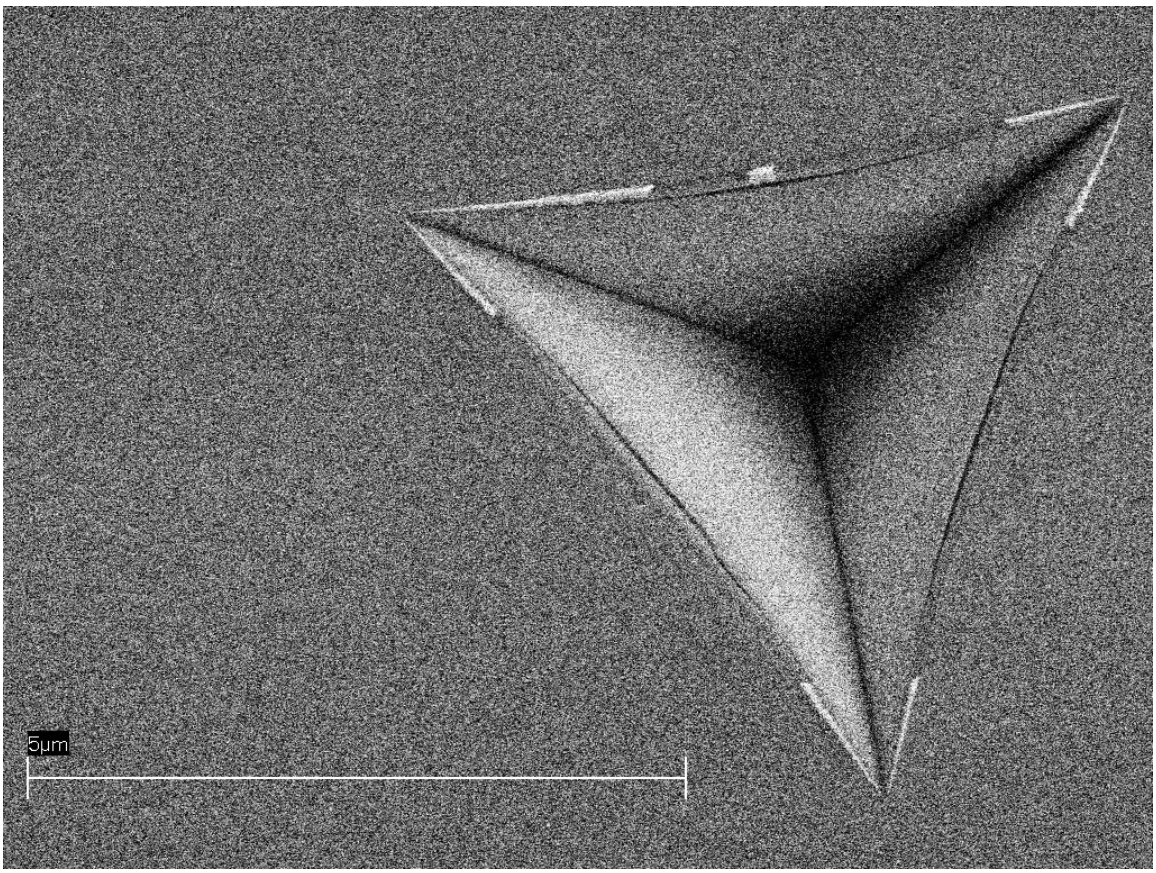

Figure 22 $\alpha = 45^{o}$ indent (P_{max} = 120mN) showing extruded gold material (white) and where the gold was removed by the indenter (darker areas between white lines)

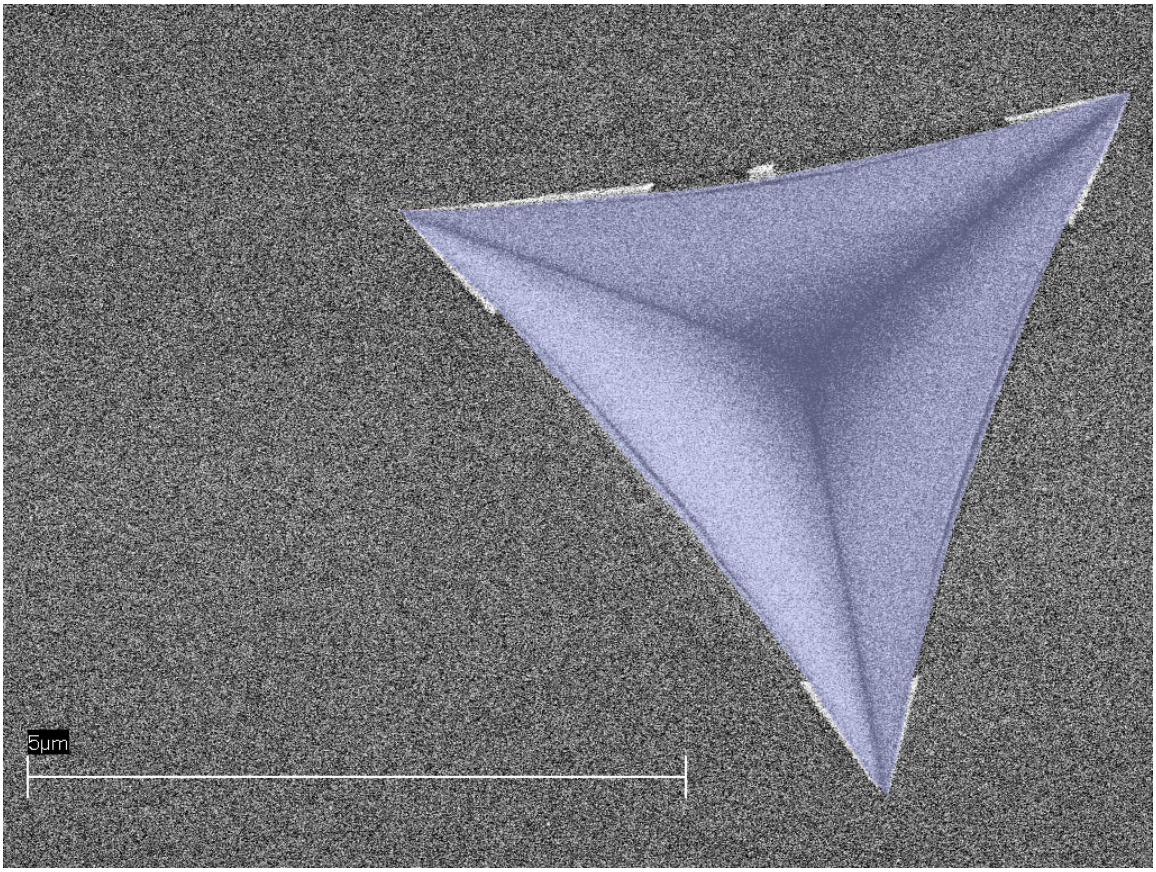

Figure 23 $\alpha = 45^{o}$ indent (P_{max} = 120mN) with colored region showing area measurement

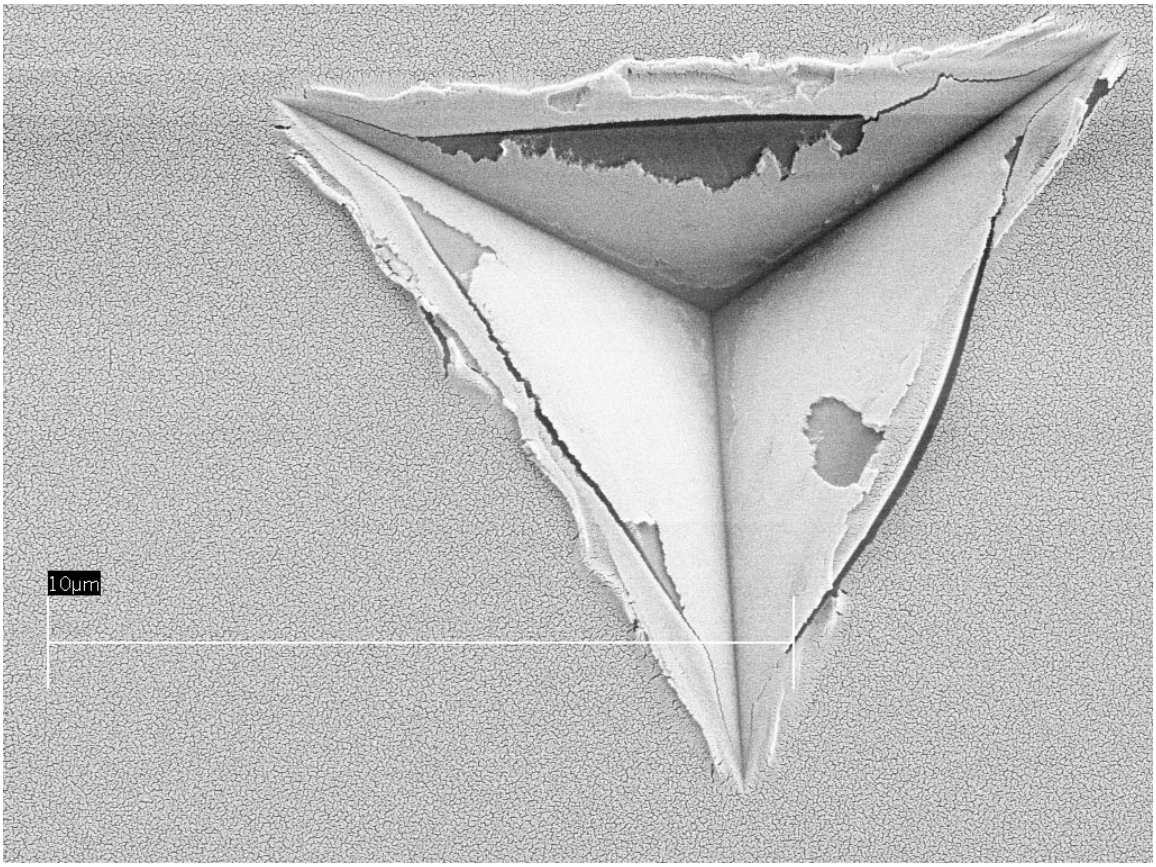

Figure 24 $\alpha = 55^{o}$ (P_{max} = 420mN) indent showing both extrusion and flattening of gold surface

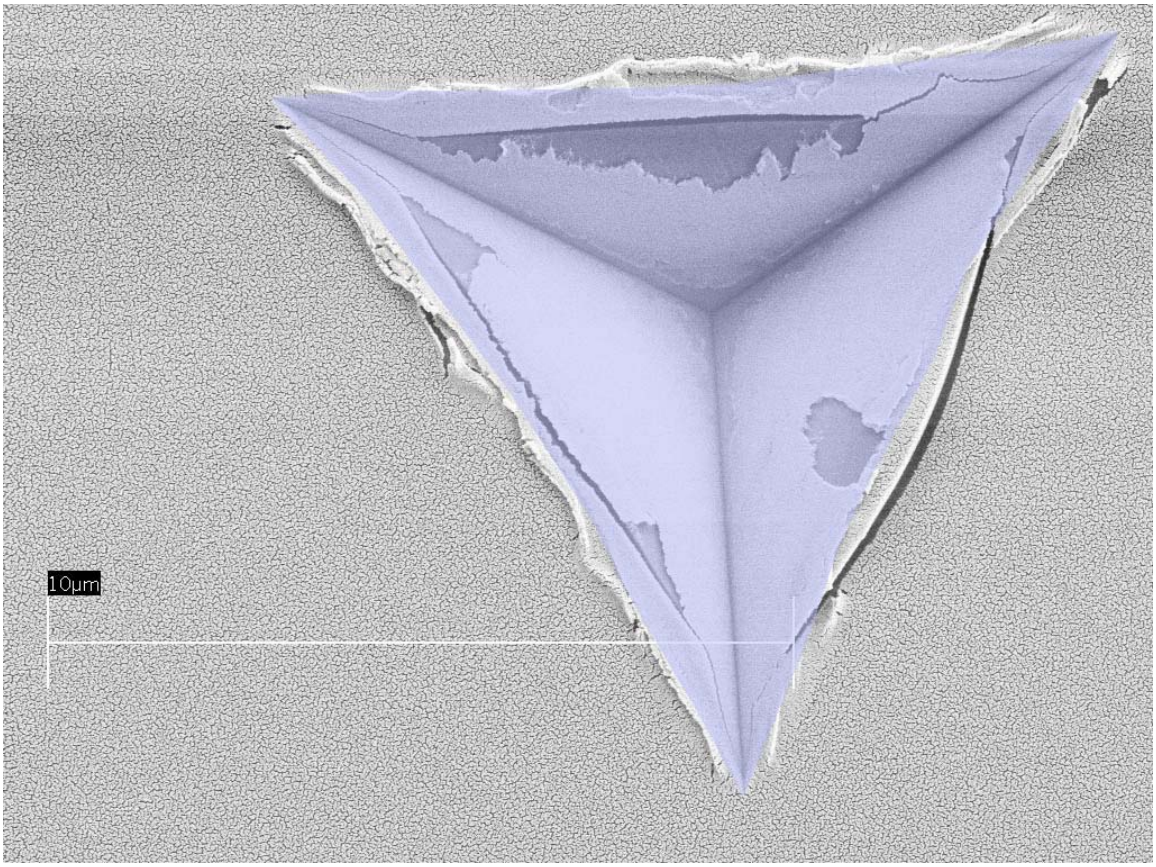

Figure 25 $\alpha = 55^{o}$ indent (P_{max} = 420mN) showing choice of contact area

2.7 Finite Element Calculations

2D and 3D finite element simulations were performed using the ABAQUS® finite element code (assisted by Dr. Sanghoon Shim). In ABAQUS®, the indenters were modeled by axisymmetric rigid cones for the 2D case. For the 3D case, a rigid ideal Berkovich pyramid and a rigid cone was used. Simulations were performed using a friction coefficient of $\mu = 0.2$ and $\mu = 0$, with an elastic-perfectly plastic constitutive law of E = 72 GPa and $\nu = 0.17$ and a yield stress of 5.5 GPa, which gives the hardness of 9.4 GPa as observed in experiments. The 3D mesh is displayed in Figure 26. An elastic-linear hardening constitutive law with E = 73.1 GPa, n = 0.13, hardening modulus of 0.1 GPa, and a yield stress of 5.7 GPa was also used in 2D experiments to confirm insensitivity to reasonable constitutive laws. All tests were run using a displacement controlled analysis. The 3D mesh was verified by comparing results from 3D conical indentations to those of 2D conical indentations which were in excellent agreement. For the case of a frictionless Berkovich indenter, calculated contact areas varied by no more than 0.3%. All analyses in this work relating to FEA will rely on the 3D pyramidal elastic-perfectly plastic simulations [8].

2.8 Error Analysis

To arrive at a final uncertainty for the value of β, the error propagation method outlined in [9] was used. The total random error was calculated in the final value of β using:

$$\delta\beta_{ran} = \sqrt{\left(\frac{\partial\beta}{\partial S}\delta S_{ran}\right)^2 + \left(\frac{\partial\beta}{\partial A_c}\delta A_{c_{ran}}\right)^2}, \qquad 11$$

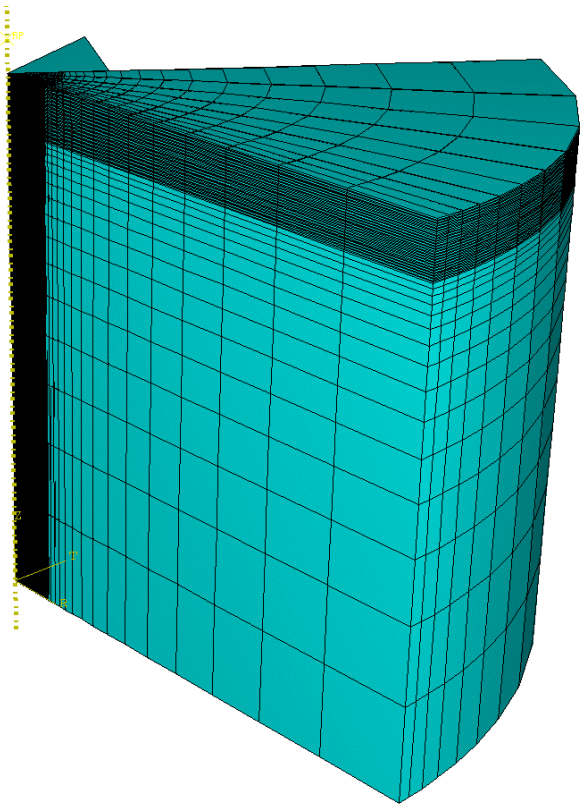

Figure 26 3D Finite element mesh

where:

$$\frac{\partial \beta}{\partial S} = \left(2E_r \sqrt{\frac{A}{\pi}} \right)^{-1}, \tag{12}$$

and,

$$\frac{\partial \beta}{\partial A} = \frac{-S}{4E_r \left(\frac{A}{\pi} \right)^{\frac{3}{2}} \pi}, \tag{13}$$

and δS_{ran} is the estimated random error observed in the stiffness measurement and $\delta A_{c_{ran}}$ is the estimated random error in the contact area measurement. The total systematic error in β is similarly calculated by:

$$\delta \beta_{sys} = \sqrt{\left(\frac{\partial \beta}{\partial S} \delta S_{sys} \right)^2 + \left(\frac{\partial \beta}{\partial A_c} \delta A_{c_{sys}} \right)^2 + \left(\frac{\partial \beta}{\partial E_r} \delta E_{r_{sys}} \right)^2}, \tag{14}$$

where:

$$\delta E_{r_{sys}} = \sqrt{\left(\frac{\partial E_r}{\partial E_s} \delta E_{s_{sys}} \right)^2 + \left(\frac{\partial E_r}{\partial \nu_s} \delta \nu_{s_{sys}} \right)^2}, \tag{15}$$

$$\frac{\partial E_r}{\partial E_s} = \frac{1 - \nu_s^2}{\left(\frac{1 - \nu_s^2}{E_s} + \frac{1 - \nu_i^2}{E_i} \right)^2 E_s^2}, \tag{16}$$

$$\frac{\partial E_r}{\partial \nu_s} = \frac{2\nu_s}{\left(\frac{1 - \nu_s^2}{E_s} + \frac{1 - \nu_i^2}{E_i} \right)^2 E_s}, \tag{17}$$

δS_{sys} is the possible systematic error in the stiffness measurement, $\delta A_{c_{sys}}$ is the possible systematic error in the contact area measurement, and $\delta E_{r_{sys}}$ is the possible systematic error in the reduced elastic modulus. $\delta E_{r_{sys}}$ may now be calculated using Eq. 15 with the elastic constants and uncertainties given in section 2.4 [10]. This calculation yields:

$$\delta \mathrm{E}_{\mathrm{r}_{\mathrm{sys}}} = 0.4\mathrm{GPa}\,. \tag{18}$$

This value will be used later to calculate the uncertainties of β for each indenter. For simplicity, the errors are sometimes combined using:

$$\delta\beta = \sqrt{\left(\delta\beta_{ran}\right)^2 + \left(\delta\beta_{sys}\right)^2}\,. \tag{19}$$

The value of β is reported in two ways. First when the notation $\beta = 1.054 \pm 0.02$ is used, the uncertainty includes both the random and possible systematic errors using Eq. 19. When the notation $\beta = 1.055 \pm 0.01 \pm 0.01$ is used, the first number is the random error, and the second number is the possible systematic error.

3 Results & Discussion

3.1 Elastic Recovery Correction

The area used in Eq. 1 is the projected contact area under load, while the area measured in the SEM was taken after unload. Figure 27a shows schematically the elastic recovery observed in conical finite element simulations. For the case of the 2D 70.3^o frictionless conical indenter, the edge of the contact moves outward during unloading, increasing the apparent contact area by 8.8%. This result agrees to within 0.2% with my 2D Elastic-Linear Hardening tests, and within 1% of the 3D conical test. For the 3D case, the simulations for a true frictionless Berkovich pyramid are shown in Figure 27b. Here, the area increases upon unloading by a slightly larger amount, 9.47% [8]. It is not clear which of these two values is the better estimate; for further evaluation, the 3D Berkovich value is used. Accordingly, the contact areas measured in SEM micrographs were corrected by assuming they are too large by 9.5%. This is accomplished using:

$$A_{cl} = \lambda A_{cu}, \qquad 20$$

where A_{cu} is the projected contact area measured after unloading, A_{cl} is the true projected contact area at full load, and λ is the correction factor given by Eq. 20. The values used for l are given in Table 3. As the indenters become sharper, friction has an increasing effect on the correction factor. The resultant correction factor used to determine β was calculated from the 3D results including a friction coefficient of μ=0.2. Detailed results of the contact edge motion for the 3D finite element simulations are presented in the appendix, Figure A-1 through Figure A-9.

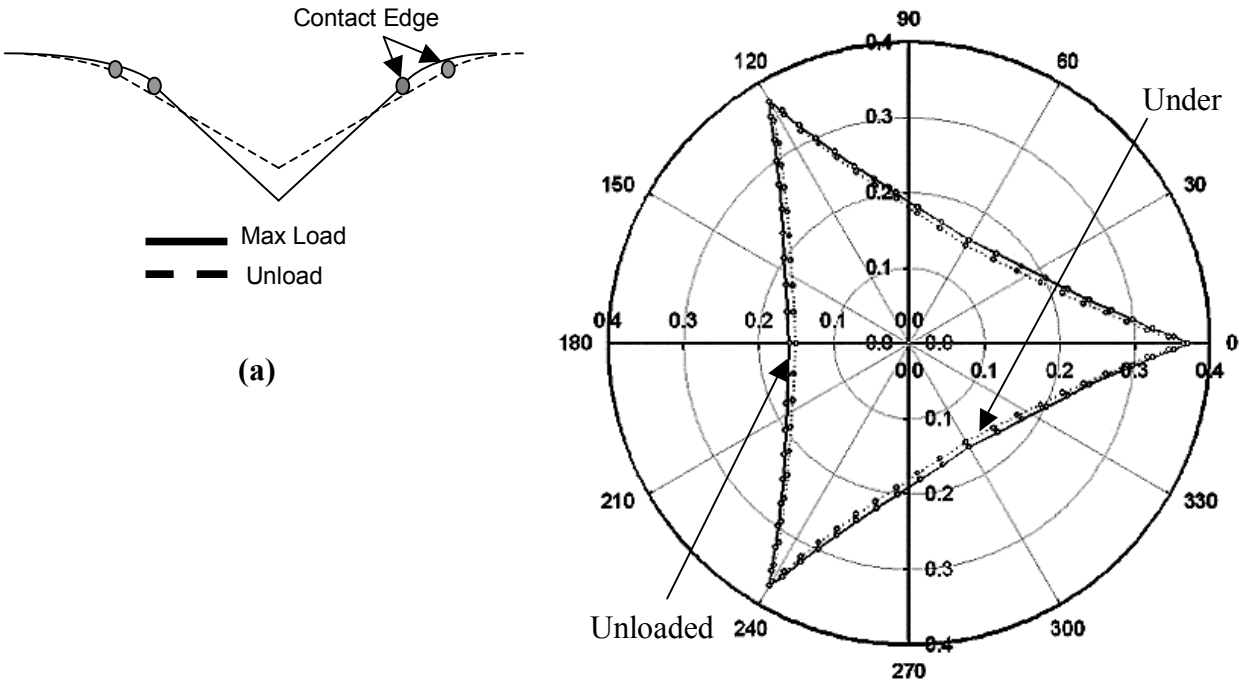

Figure 27 Finite element simulation results showing increase in apparent contact area due to elastic recovery during unloading: (a) schematic of 2D conical simulations; (b) 3D simulations of a true Berkovich indenter

Table 3 FEA Results: Contact area change (Sanghoon Shim)

Indenter Angle α	Friction Coefficient	2D	3D
		λ	λ
35.3°	μ=0	0.971	1.068
	μ=0.2	0.912	0.973
45°	μ=0	0.935	0.974
	μ=0.2	0.912	0.939
55°	μ=0	0.907	0.933
	μ=0.2	0.914	0.919
65.3°	μ=0	0.920	0.913
	μ=0.2	0.920	0.912
75°	μ=0	0.933	0.928
	μ=0.2	0.934	0.928
85°	μ=0	0.996	0.971
	μ=0.2	0.996	0.972

3.2 Effect of Gold Coating

The effects of the gold coating on the measurements must now be investigated. The gold coating has a pronounced effect at small depths, but diminishes as the test proceeds to larger depths. This can be seen in Figure 28, Figure 29, and Figure 32, where a number of Berkovich indents are compared with data shown from the 11nm gold coated region on the sample (red), and an uncoated region nearby (blue). Figure 30 shows clearly that at smaller depths the gold coating has a pronounced effect on the stiffness measurement, but the depths used in this study the differences in stiffness between the coated and uncoated lie well within the noise produced by the machine as is shown in Figure 31. One can see almost no difference for the load-displacement curves, but for the parameter P/S^2 (which should be flat assuming load frame compliance is accurate and constant hardness) there is divergence at small depths that disappears as the depth exceeds about 1500nm. Similarly the load-displacement and the stiffness-displacement curves are shown for the 75° indenter for coated and uncoated tests in Figure 33 and Figure 34. The only set of tests that did not exceed a depth of 1500nm were the $\phi = 85^{o}$ indents which penetrated to a depth of 700nm. A comparison of the contact stiffness versus depth is shown in Figure 35 showing the difference between the 11nm coated surface (red) and the uncoated surface (blue). This plot suggests that the presence of the gold coating has little or no affect on the $\phi = 85^{o}$ tests save the surface find. Table 4 shows depths and stiffnesses of representative indents in gold-coated and adjacent uncoated fused quartz demonstrating the negligible effect the gold coating has on

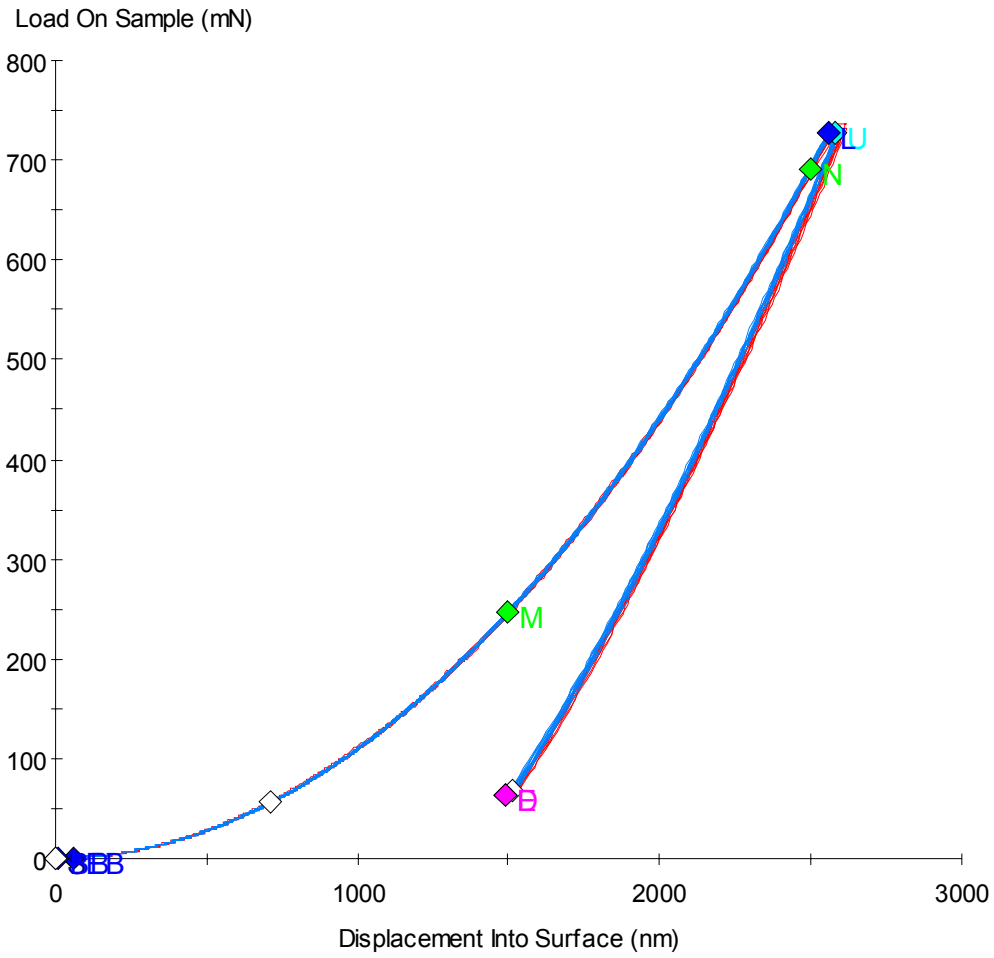

Figure 28 Load vs. displacement curve for Berkovich indents. red = 11nm coating, blue = uncoated.

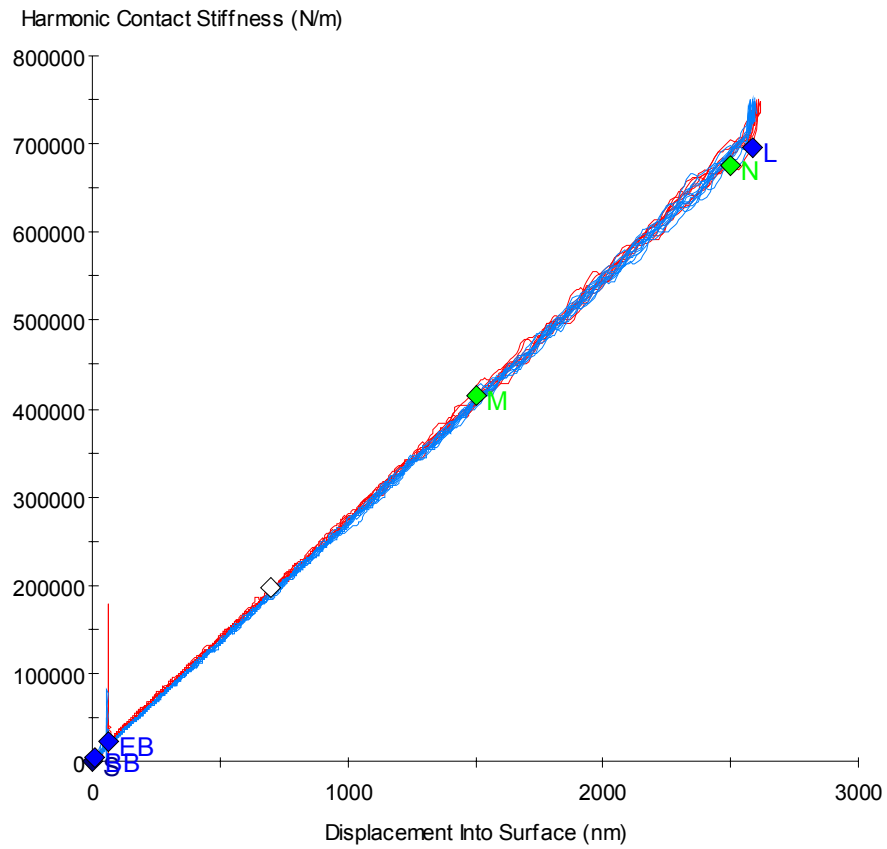

Figure 29 Berkovich harmonic contact stiffness vs. displacement red = 11nm coating, blue = uncoated

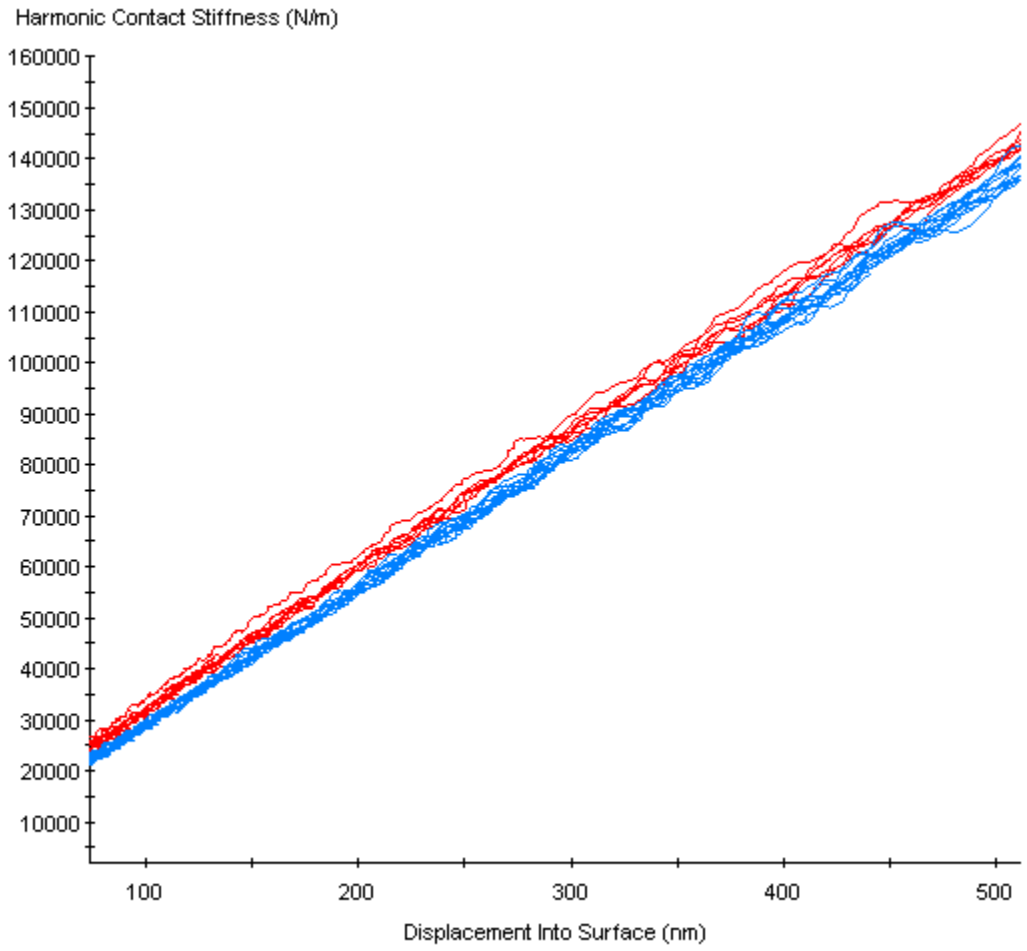

Figure 30 Small depths: Berkovich harmonic contact stiffness vs. displacement red = 11nm coating, blue = uncoated

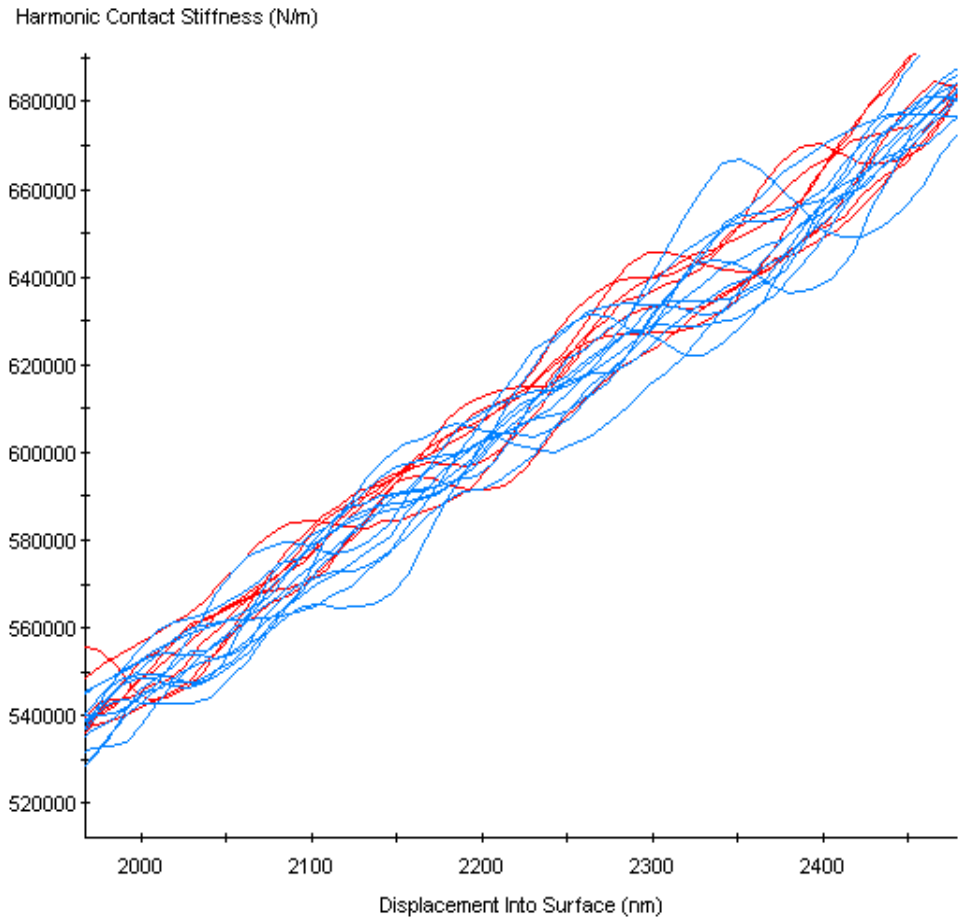

Figure 31 Large depths: Berkovich harmonic contact stiffness vs. displacement red = 11nm coating, blue = uncoated

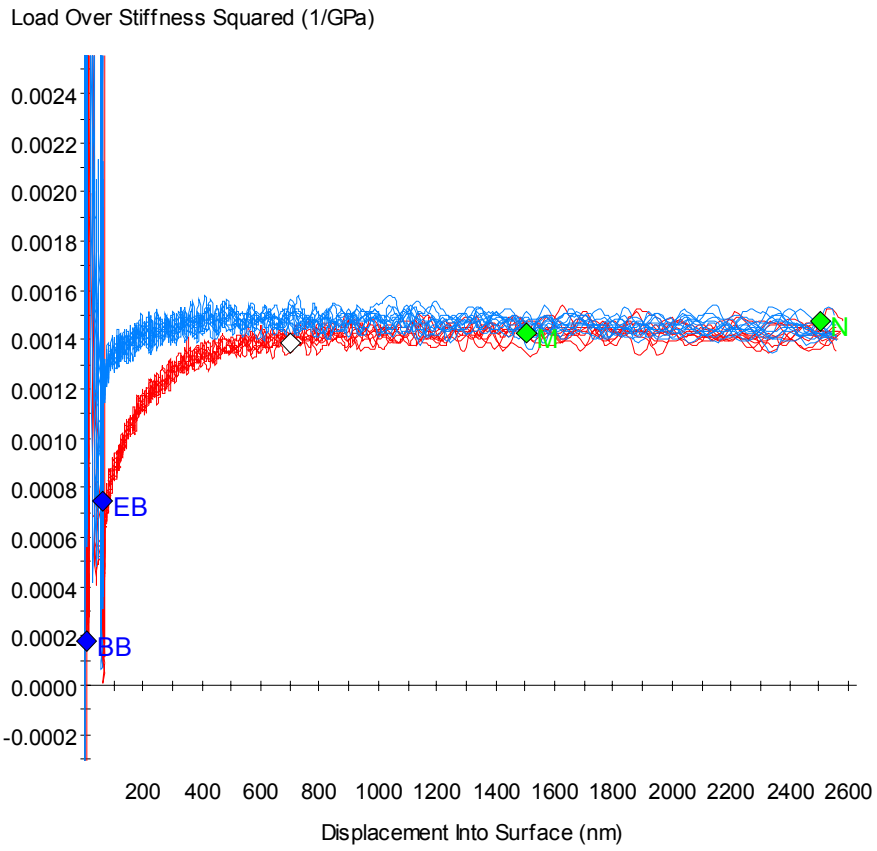

Figure 32 Berkovich load over stiffness squared vs. displacement red = 11nm coated, blue = uncoated

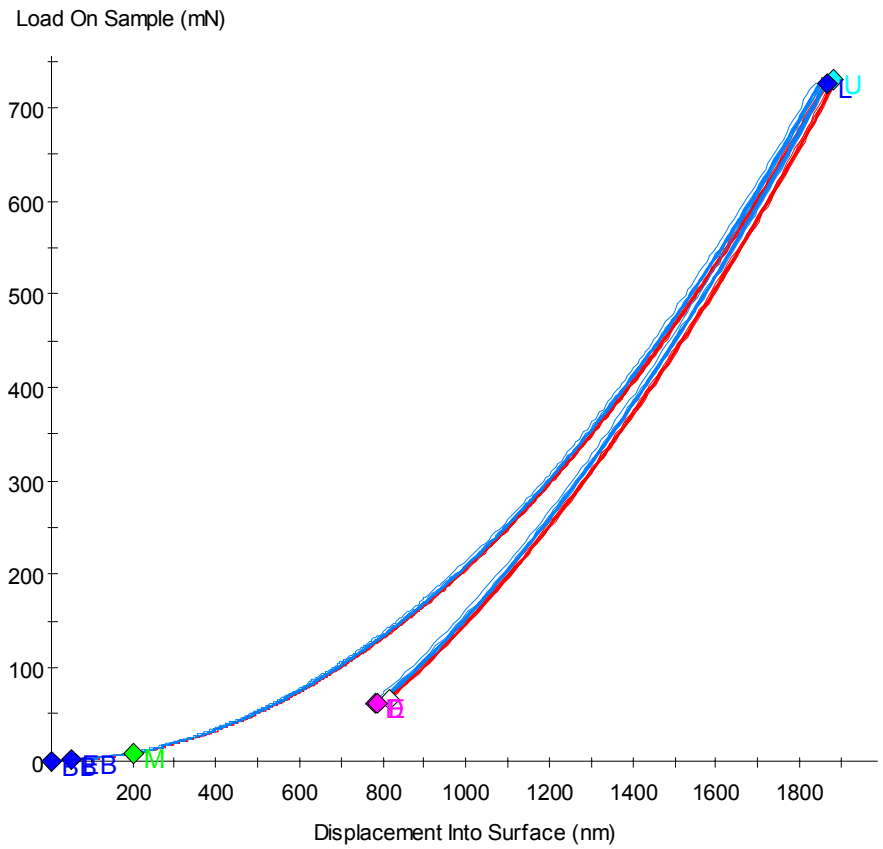

Figure 33 75^{o} Load vs. displacement red = 11nm coated, blue = uncoated

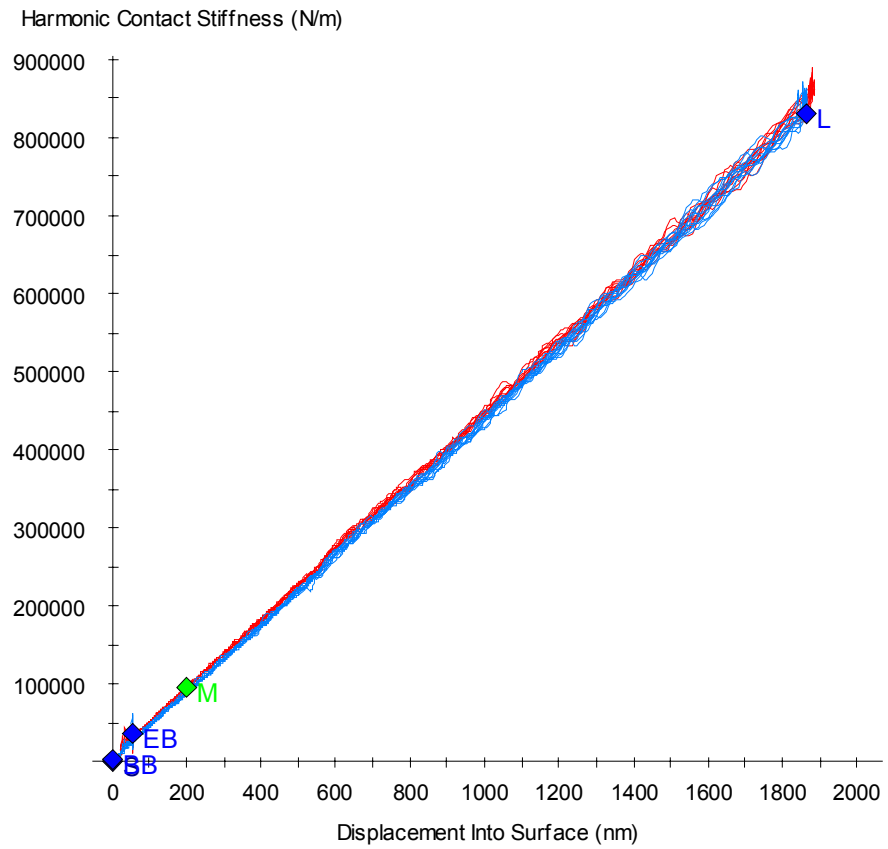

Figure 34 75° Stiffness vs. displacement red = 11nm coated, blue = uncoated

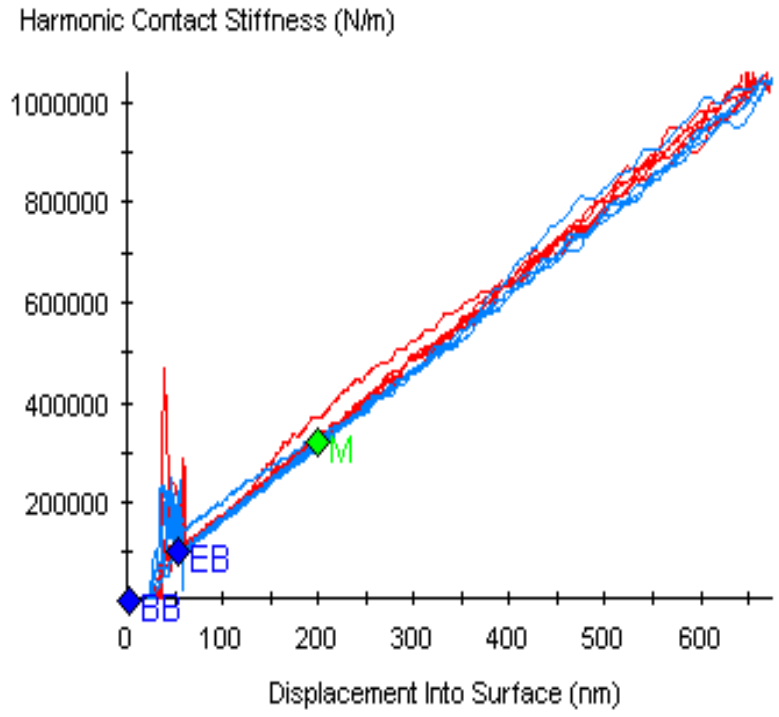

Figure 35 85^{o} Harmonic contact stiffness vs. displacement red = 11nm coated, blue = uncoated

Table 4 Comparison of indents in coated and adjacent uncoated regions of fused quartz

	Coated		Uncoated	
Indenter Angle	Maximum Depth	Stiffness	Maximum Depth	Stiffness
(degrees)	(nm)	(N/m)	(nm)	(N/m)
35	2004	234000	1999	233000
35	1993	241000	1986	237000
45	1744	287000		
45	1747	287000	No data available	
55	2586	537000	2557	530000
55	2583	541000	2551	521000
65	2594	742000	2593	742000
65	2585	734000	2584	736000
75	1883	861000	1858	844000
75	1887	866000	1863	845000
85	656	1050000	656	1015000
85	657	1057000	656	1047000

measured stiffness. Slightly different maximum depths between the coated and uncoated indents account from most of the variation in measured stiffness.

3.3 Calculation of β

From the independent measurements of S, A_c, and E_r and accounting for the elastic recovery upon unloading, Eq. 1 yields a value of $\beta = 1.055$ for Berkovich indentation of fused quartz. The standard deviation based on seven separate measurements is ±0.011. The results for all indenters are summarized in Figure 36 with the error bars indicating one standard deviation from the mean. The individual test results are given in Table 5 with the hardness reported being the hardness after correction for lateral contraction.

In addition to measuring β directly from experiments, the dependence of β on indenter angle was also measured from the 2D and 3D FEA analysis for a purely elastic medium is shown Figure 37, and the elastic perfectly plastic case is shown in Figure 38 [8].

3.4 Error Analysis

3.4.1 Systematic Error

Systematic error appears in all the variables needed to calculate β. The value for the possible systematic error in E_r has already been arrived at in Eq. 18 which gives us Er = 69.8 $\pm$ 0.4 GPa. Next, one must look at the contact area. There are two sources of error which may be combined by using Eq. 19. The uncertainty in the correction factor λ is estimated to give us no more than a 2% error in the area measurement for indenters of

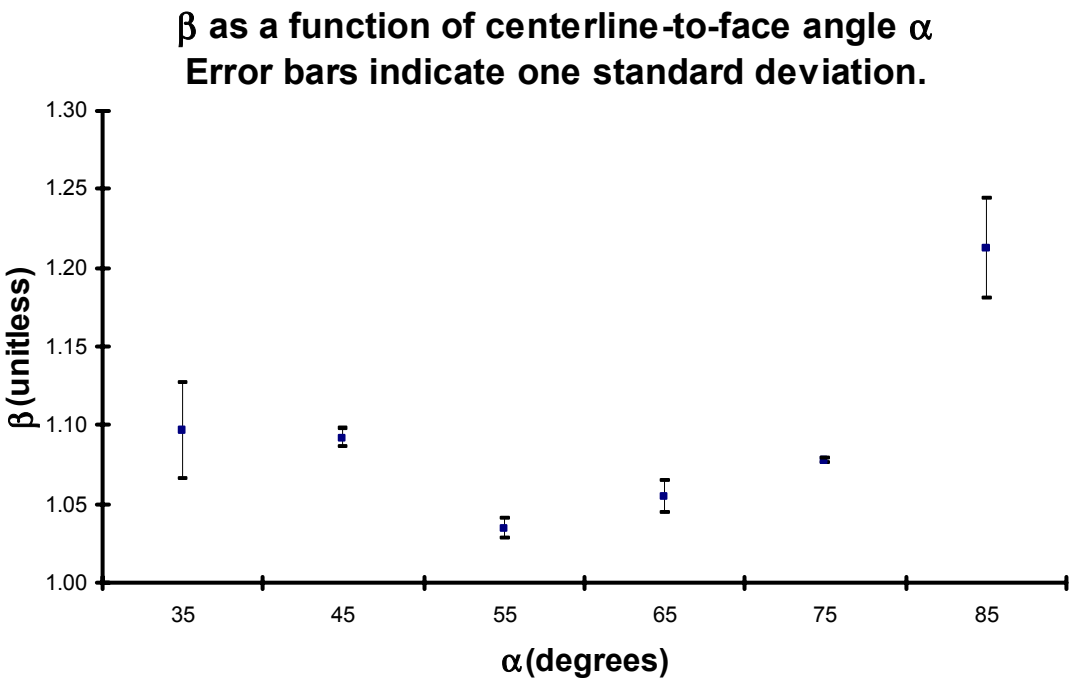

Figure 36 β vs. Indenter angle α. error bars indicate one standard deviation

Table 5 Individual test results

Indenter degrees	Area μm	Max Load mN	Displacement nm	Stiffness N/m	Hardness GPa	β
35	8.08	81.6	2004	234500	10.10	1.062
35	7.85	82.5	1993	241400	10.51	1.109
35	7.76	82.2	1998	242000	10.60	1.118
45	11.86	121.8	1744	286600	10.27	1.090
45	11.98	122.3	1747	287200	10.21	1.086
45	12.10	123.0	1752	291500	10.17	1.097
55	48.10	417.8	2586	537300	8.69	1.026
55	47.30	418.4	2583	540800	8.85	1.041
55	48.10	419.6	2582	541700	8.72	1.034
55	48.00	419.5	2581	541400	8.74	1.035
65	86.07	729.9	2577	733700	8.48	1.051
65	88.50	729.5	2598	752000	8.24	1.062
65	86.60	729.7	2594	742300	8.43	1.060
65	86.88	728.2	2585	733700	8.38	1.046
65	85.45	727.5	2591	744700	8.51	1.070
65	88.19	731.5	2609	739800	8.29	1.047
65	87.64	729.3	2601	733700	8.32	1.041
75	111.32	730.1	1891	863700	6.56	1.078

Table 5 Continued

Indenter degrees	Area μm	Max Load mN	Displacement nm	Stiffness N/m	Hardness GPa	β
75	111.68	729.1	1977	863700	6.53	1.077
75	111.00	727.3	1883	861100	6.55	1.077
75	112.40	733.9	1887	866200	6.53	1.076
75	111.38	727.2	1891	862400	6.53	1.076
85	122.79	308.3	648	1047700	2.51	1.217
85	118.90	313.1	656	1050400	2.63	1.240
85	133.74	311.4	657	1057000	2.33	1.177

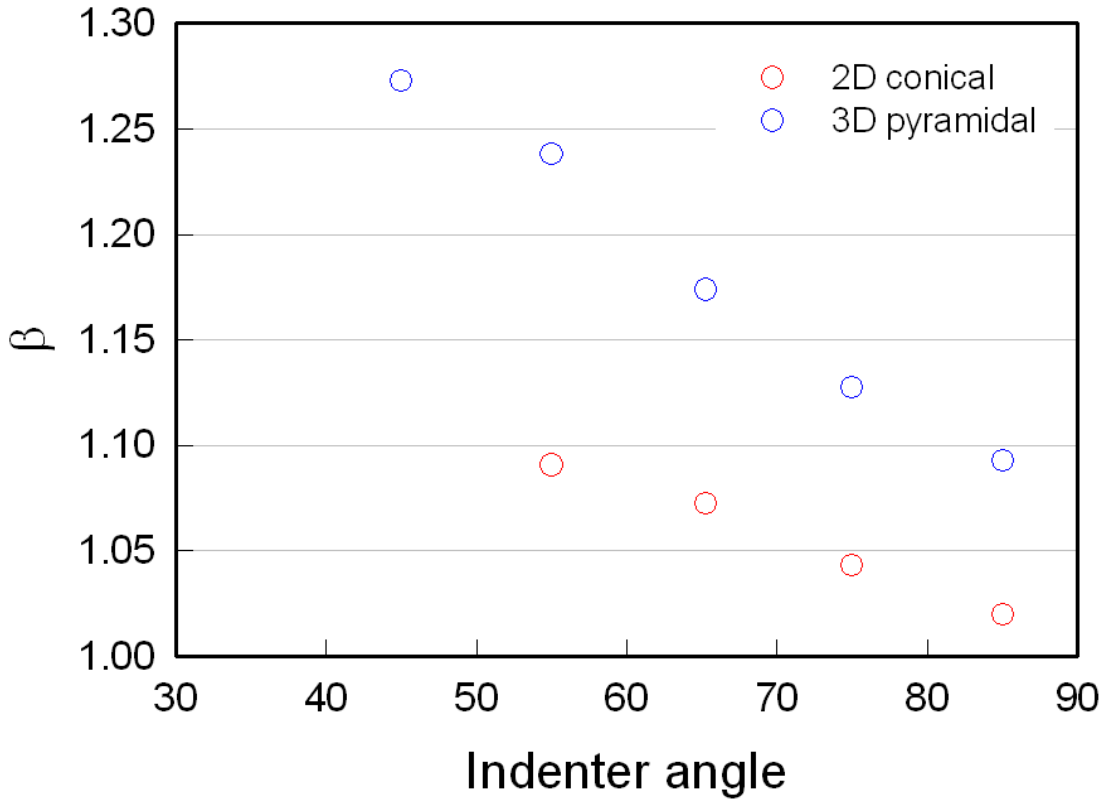

Figure 37 FEA β vs. indenter angle, elastic

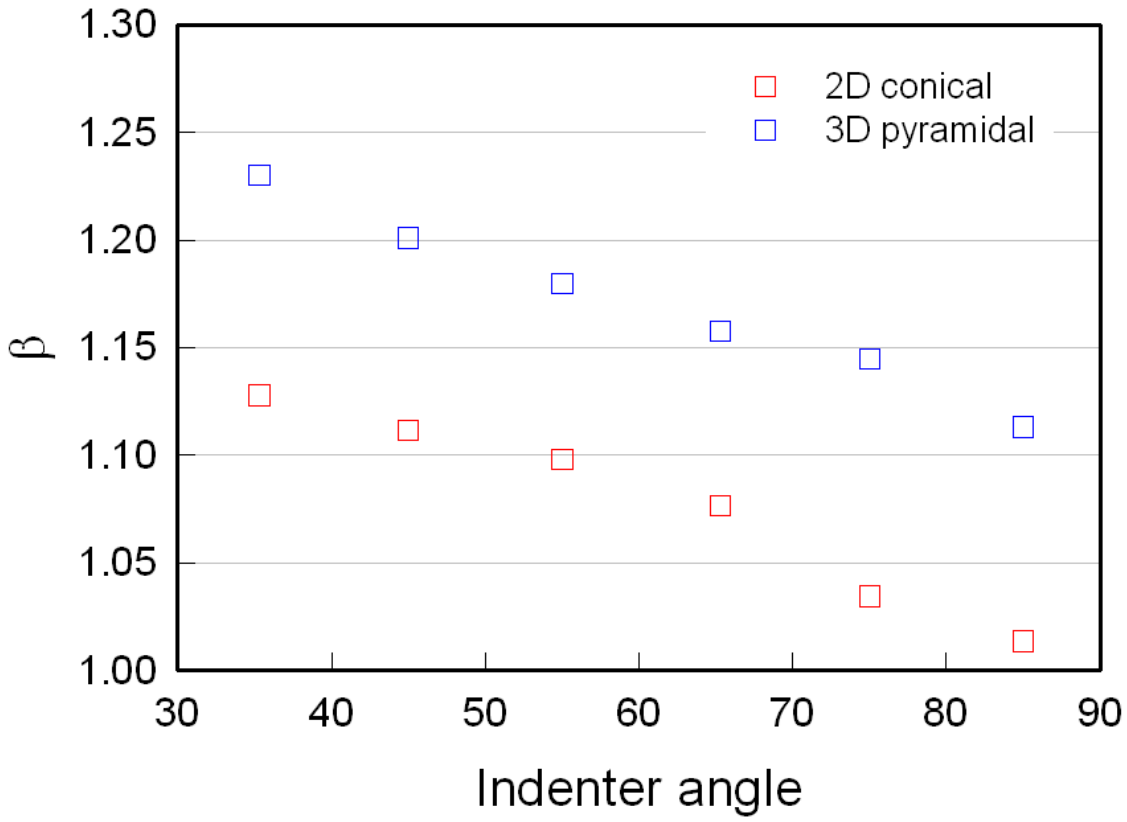

Figure 38 FEA β vs. indenter angle, elastic-perfectly plastic

$\alpha \geq 55^{o}$. The 45^{o} indenter is assumed to give at most a 3% error, and the 35^{o} indenter is assumed to give a 5% error. The assumed error is larger for the small angle indenters due to the larger change in the values of λ given in Table 3 depending on friction whether the simulation is 2D or 3D. In addition, error in the magnification resulting from the calibration of the latex spheres may yield up to a 2% error in the area measurement. Finally, one must look at the systematic error in the variable *S*. The main cause of error in *S* is the choice of the machine compliance C_m which alters the stiffness by Eq. 8. Comparing all reasonable choices of *Cm* yields a maximum systematic error in the stiffness of 0.5%.

3.4.2 Random Error

Random error must be considered when looking at observed values of contact area and harmonic stiffness. Random error in the contact area appears mostly from the inability to exactly measure the contact area from the photos taken. The value of δA_{ran} is different for the various indenters. For the cases of the indenters with $\alpha = 45$, 65 and 75, δA_{ran} was chosen to be 2% by examining the largest and the smallest contact areas. The cube-corner indenter was given a value of δA_{ran} of 5% because cracking near the contact edge made determination of the contact area more difficult. The $\alpha = 85^{o}$ indenter was also given a value of δA_{ran} of 5% due to difficulty in finding the point where the cracks in the gold surface were completely smoothed. Finally, the $\alpha = 55^{o}$ indenter was given a value of δA_{ran} of 4%*A* due to extrusion of gold material near the contact edge. The

amount of random error in the stiffness measurement due to noise is well approximated by taking 1% of the measured stiffness value.

Now that the uncertainties in each variable are known, Eqs. 11 - 17 may be used to calculate the systematic and random uncertainties in the value of β. These results are summarized in Table 6. Also, the standard deviations are compared with the values of the random error in Table 6 showing the theoretical values for $\delta\beta_{ran}$ meet or exceed those observed during testing, suggesting that the actual accuracy may be better than predicted. Table 7 shows the calculated values of β with their respective error values. The error on the right hand column represents the combined error using Eq. 19.

3.5 Load Displacement Curves

Looking at the load displacement curves of the various indenters used provides insight into the modes of deformation for each case. First, the load-displacement curve of the 85^o indent in Figure 39 shows total elastic recovery. This can be seen in Figure 40 where the only visible remnant of the indentation is the deformation in the gold coating. Plasticity begins with the 75^o indenter showing a mismatch between the loading and the unloading curves in Figure 41, and the beginnings of cracking that most likely occur upon unloading as shown in Figure 42. As expected, the trend of increasing plasticity continues as the centerline-to-face angle of the indenters decrease, also the edge cracking grows more pronounced and moves out towards the contact edge as can be seen in Figure 43 through Figure 50. For the case of $\alpha \leq 45^o$ (see Figure 48), the edge cracks nearly coincide with the edge of contact suggesting they form immediately upon unloading. Figure 51 shows the amount of relative plasticity in the sample by plotting h_f(final

Table 6 Summary of error calculations

Systematic Error						
Variable Cause	35.3°	45°	55°	65.3°	75°	85°
δA_{sys} Magnification/Gold	$0.01A_c$	$0.01A_c$	$0.01A_c$	$0.01A_c$	$0.01A_c$	$0.05A_c$
δA_{sys} λ	$0.05A_c$	$0.03A_c$	$0.01A_c$	$0.01A_c$	$0.01A_c$	$0.01A_c$
δS_{sys} Machine compliance Cm	$0.005S$	$0.005S$	$0.005S$	$0.005S$	$0.005S$	$0.005S$
δEr_{sys} Ultrasonic measurement of elastic properties	0.4 GPa	0.4 GPa	0.4 GPa	0.4 GPa	0.4 GPa	0.4 GPa
$\delta\beta_{sys}$	0.031	0.021	0.014	0.014	0.015	0.06
Random Error						
Variable Cause	35.3°	45°	55°	65.3°	75°	85°
δA_{ran} Difficulty measuring contact edge.	$0.05A_c$	$0.02A_c$	$0.04A_c$	$0.02A_c$	$0.02A_c$	$0.02A_c$
δS_{ran} Noise	$0.01S$	$0.01S$	$0.01S$	$0.01S$	$0.01S$	$0.01S$
$\delta\beta_{ran}$	0.030	0.015	0.023	0.015	0.015	0.016
σ of Calculated values of β	0.030	0.006	0.006	0.010	0.0008	0.011
Total Error						
	35.3°	45°	55°	65.3°	75°	85°
$\delta\beta$	0.043	0.026	0.027	0.021	0.021	0.062

Table 7 Calculated values of β and errors in β

Indenter angle		Random Error From Eq. 11	Systematic Error From Eq. 14	Total Error From Eq. 19
35.3^o	$\beta = 1.097$	± 0.030	± 0.031	± 0.043
45^o	$\beta = 1.092$	± 0.015	± 0.021	± 0.026
55^o	$\beta = 1.035$	± 0.023	± 0.014	± 0.027
65.3^o	$\beta = 1.055$	± 0.015	± 0.014	± 0.021
75^o	$\beta = 1.077$	± 0.015	± 0.015	± 0.021
85^o	$\beta = 1.21$	± 0.016	± 0.060	± 0.062

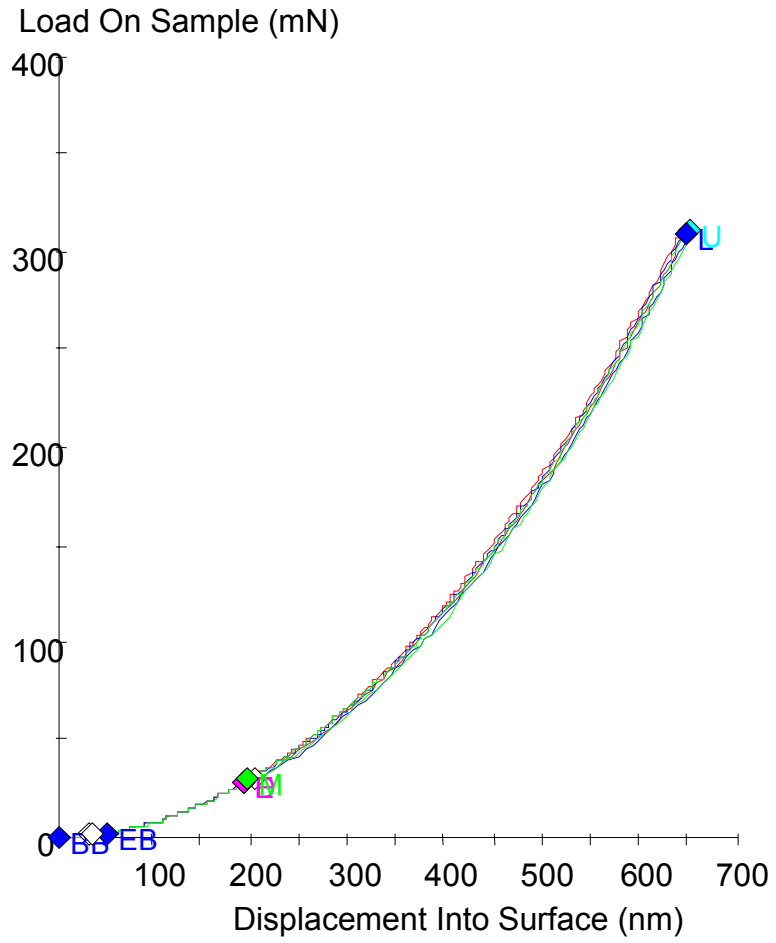

Figure 39 Load vs. displacement for 85^{o} indents

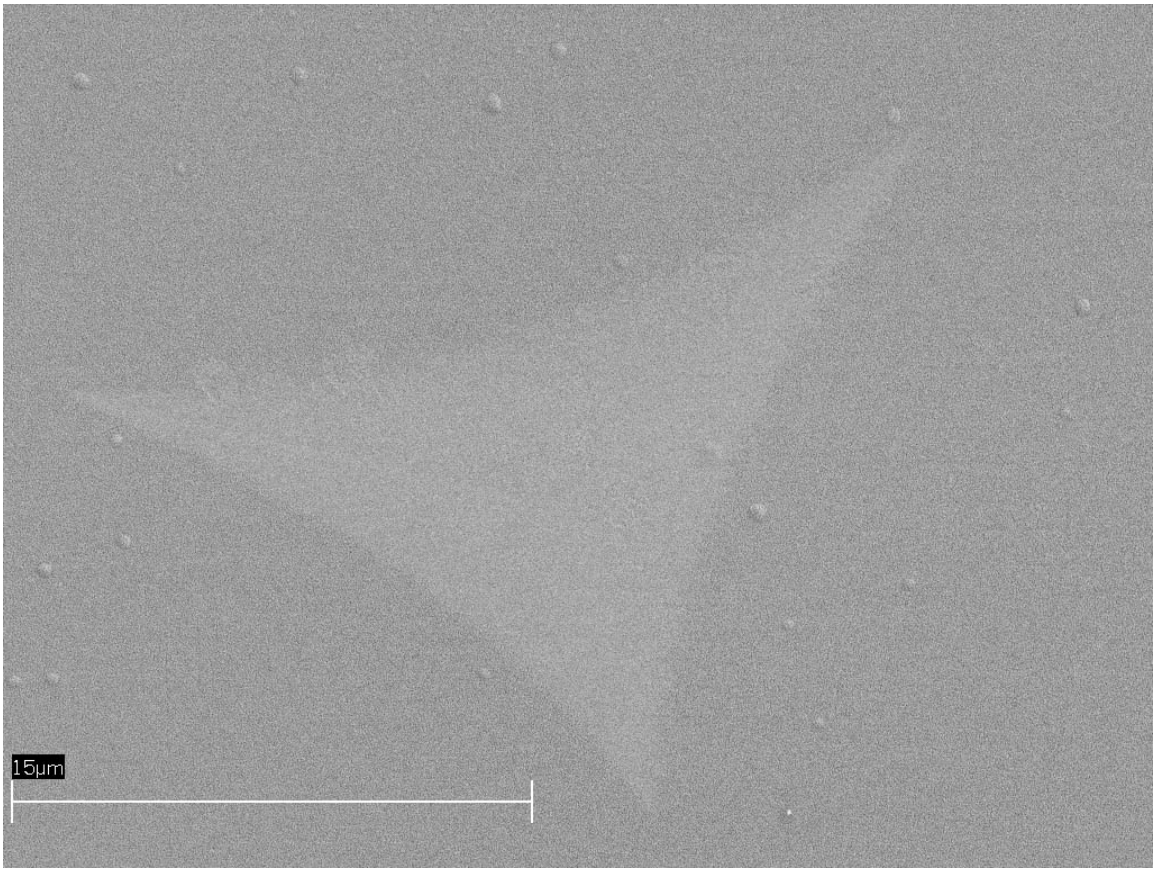

Figure 40 SEM image of 85^{o} indent

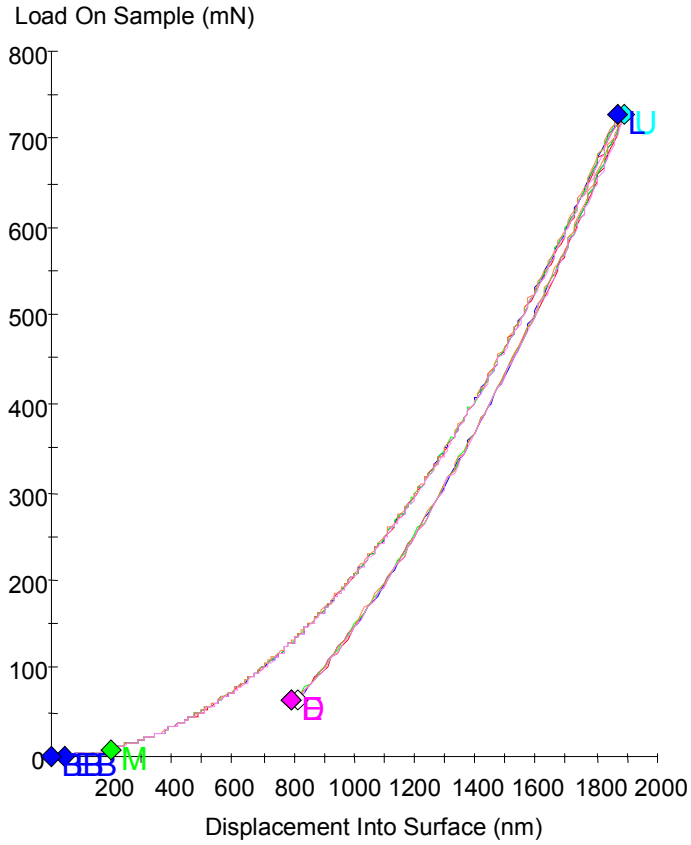

Figure 41 Load vs. displacement for 75^{o} indents

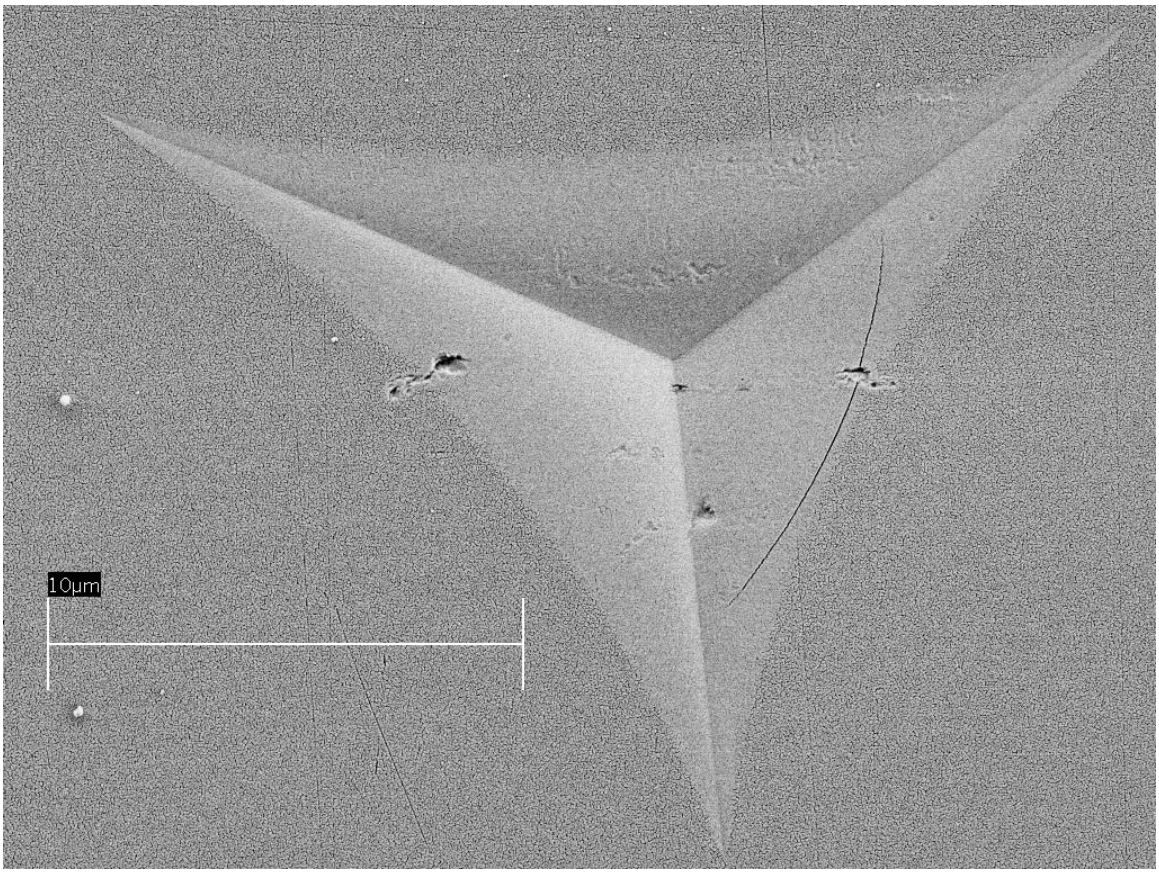

Figure 42 SEM image of 75^{o} indent

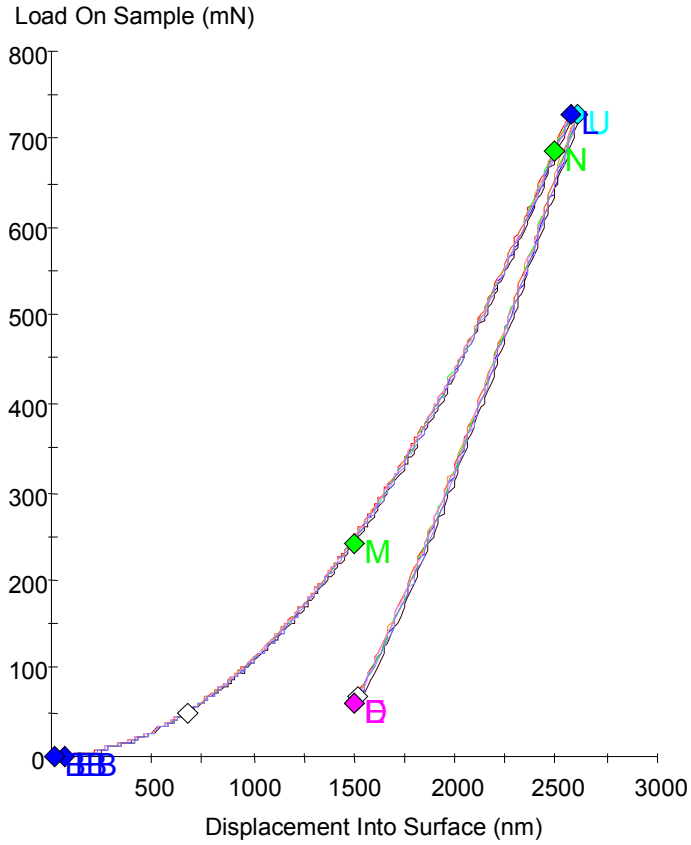

Figure 43 Load vs. displacement for 65.3° indents

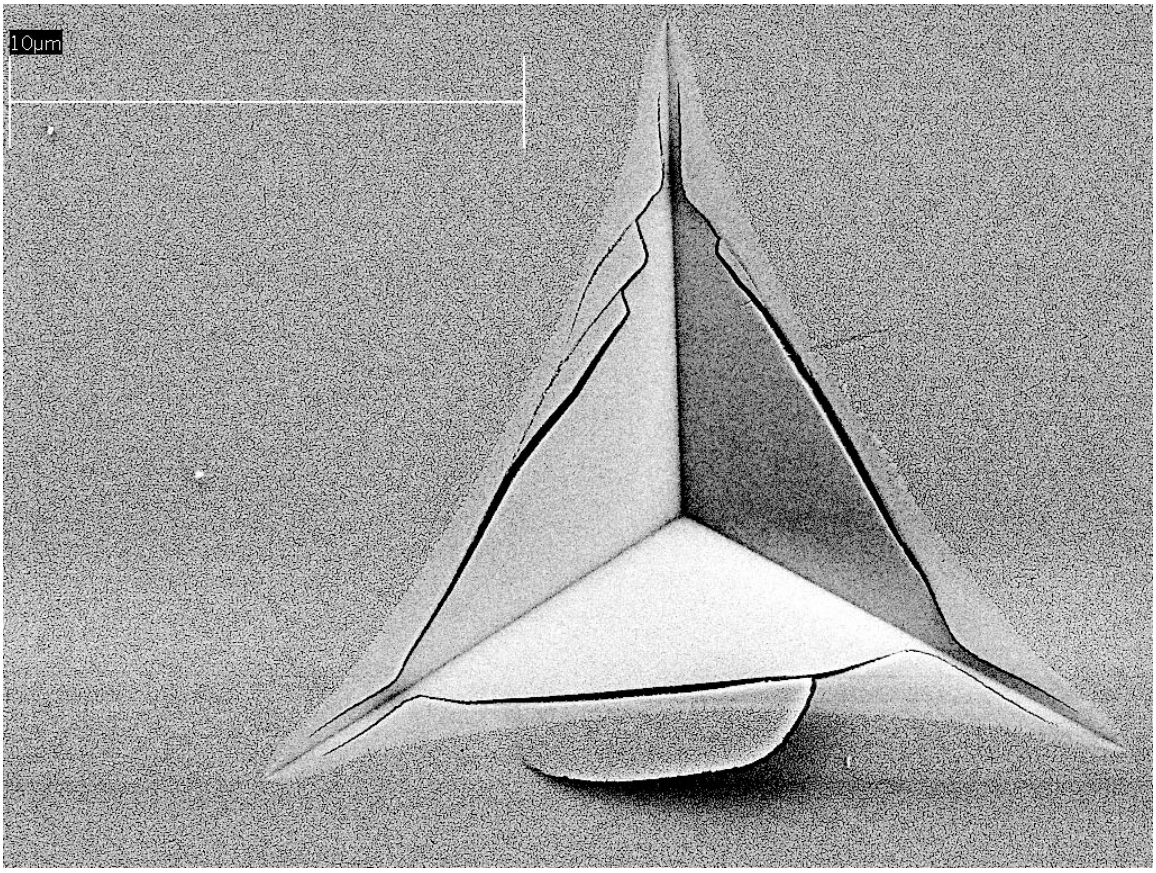

Figure 44 SEM image of 65.3^{o} indent

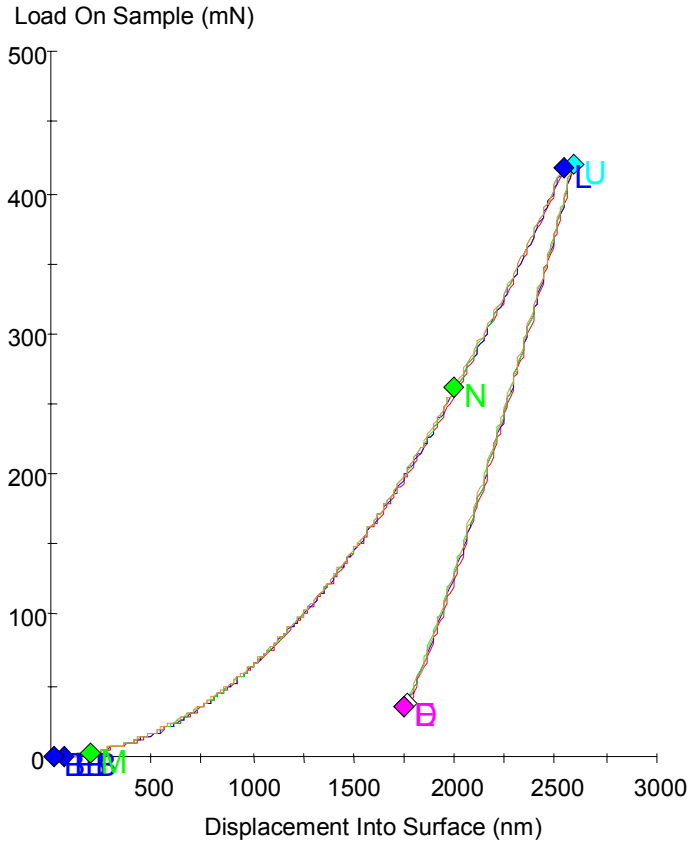

Figure 45 Load vs. displacement for 55^{o} indents

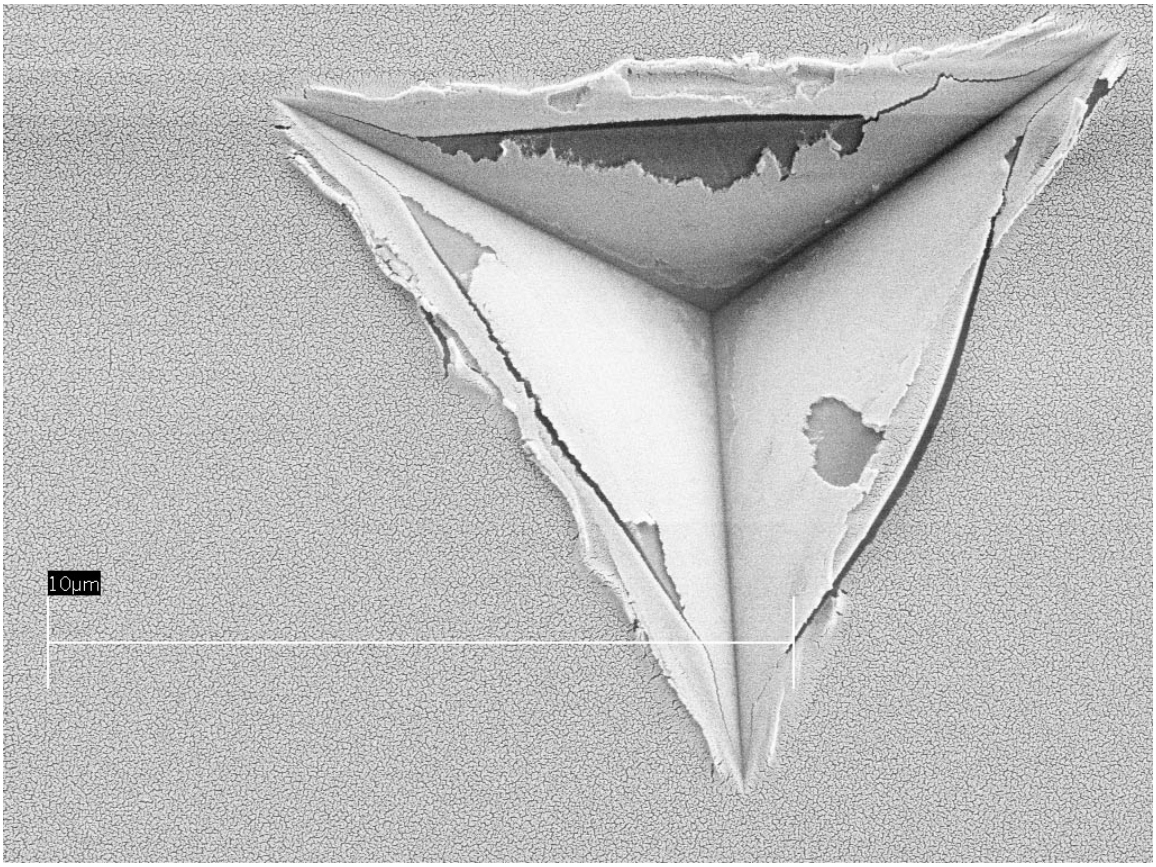

Figure 46 SEM image of 55^{o} indent

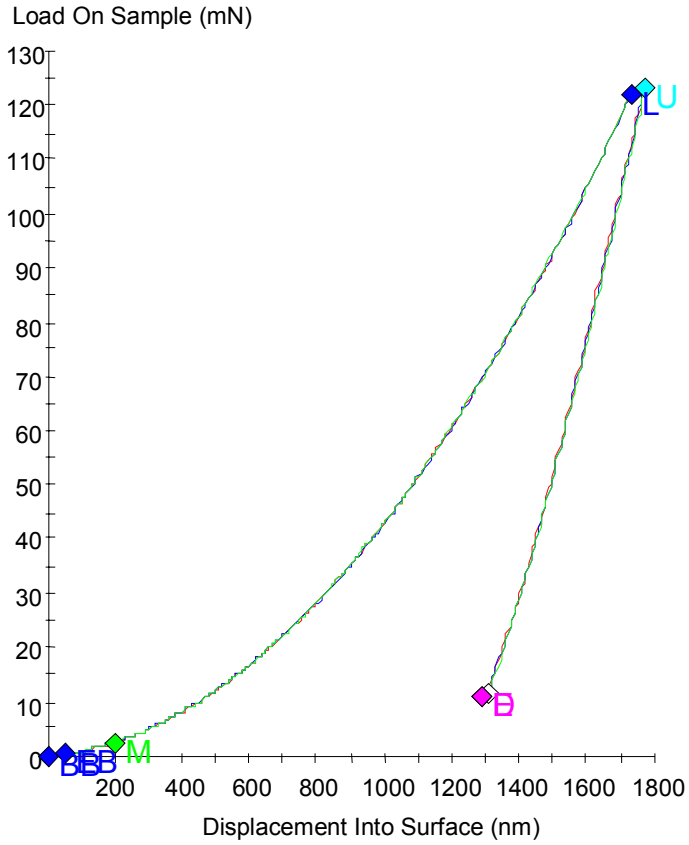

Figure 47 Load vs. displacement for 45^{o} indents

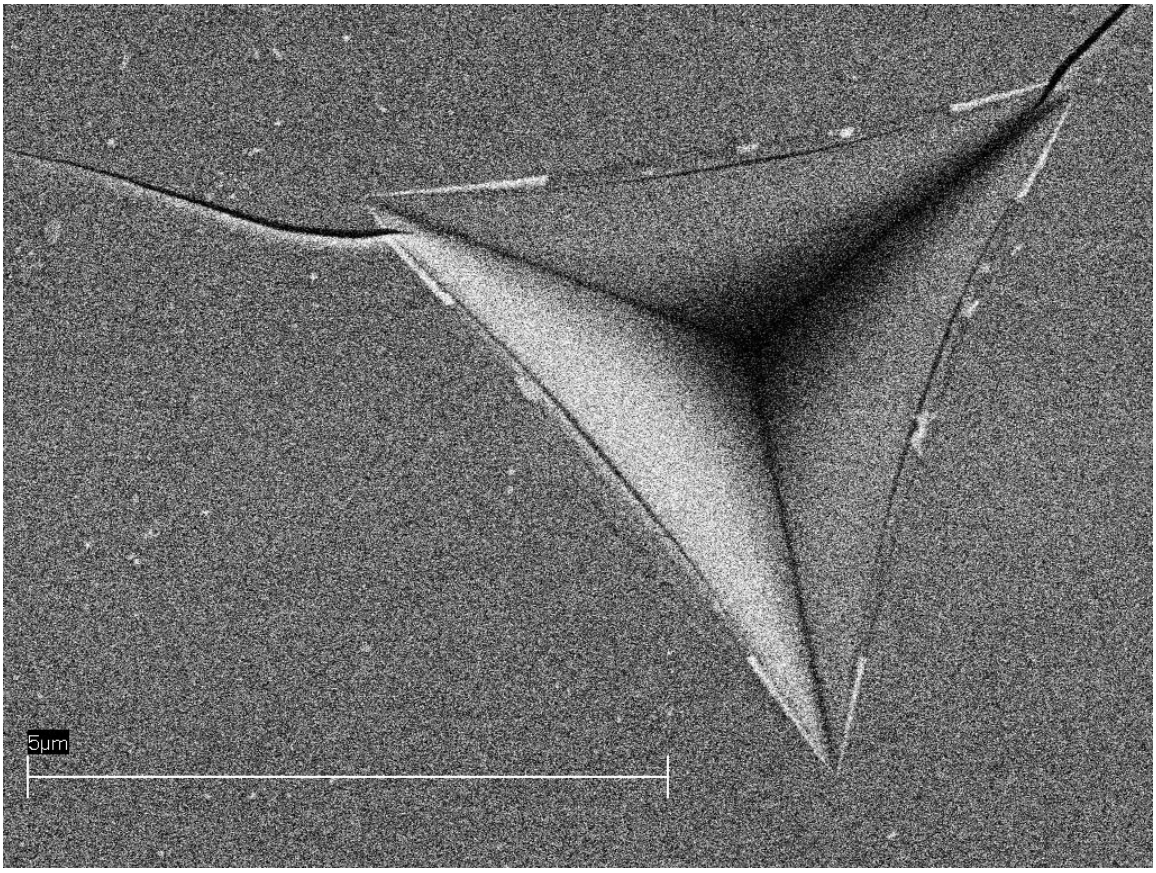

Figure 48 SEM image of 45^{o} indent

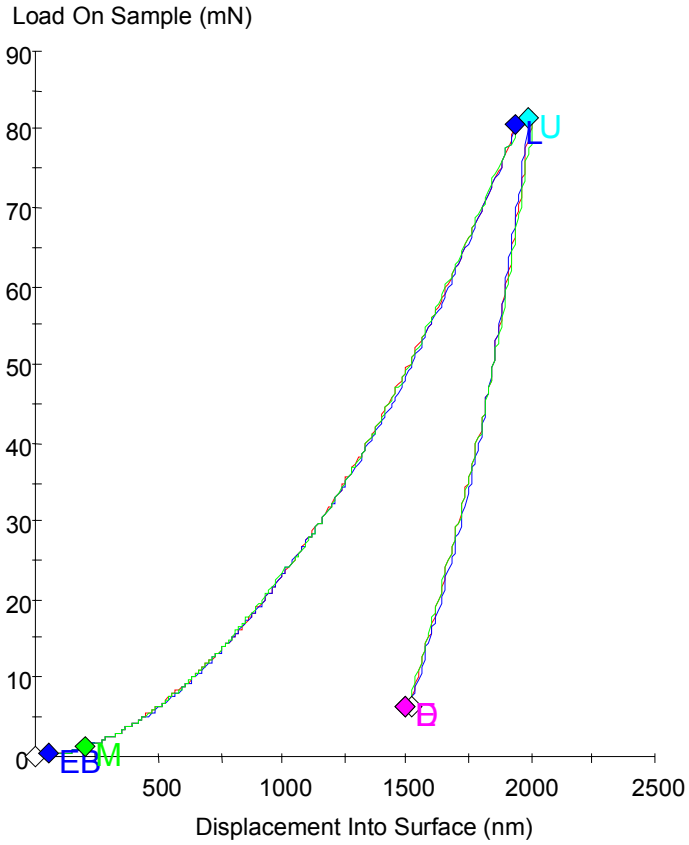

Figure 49 Load vs. displacement for 35.3° indents

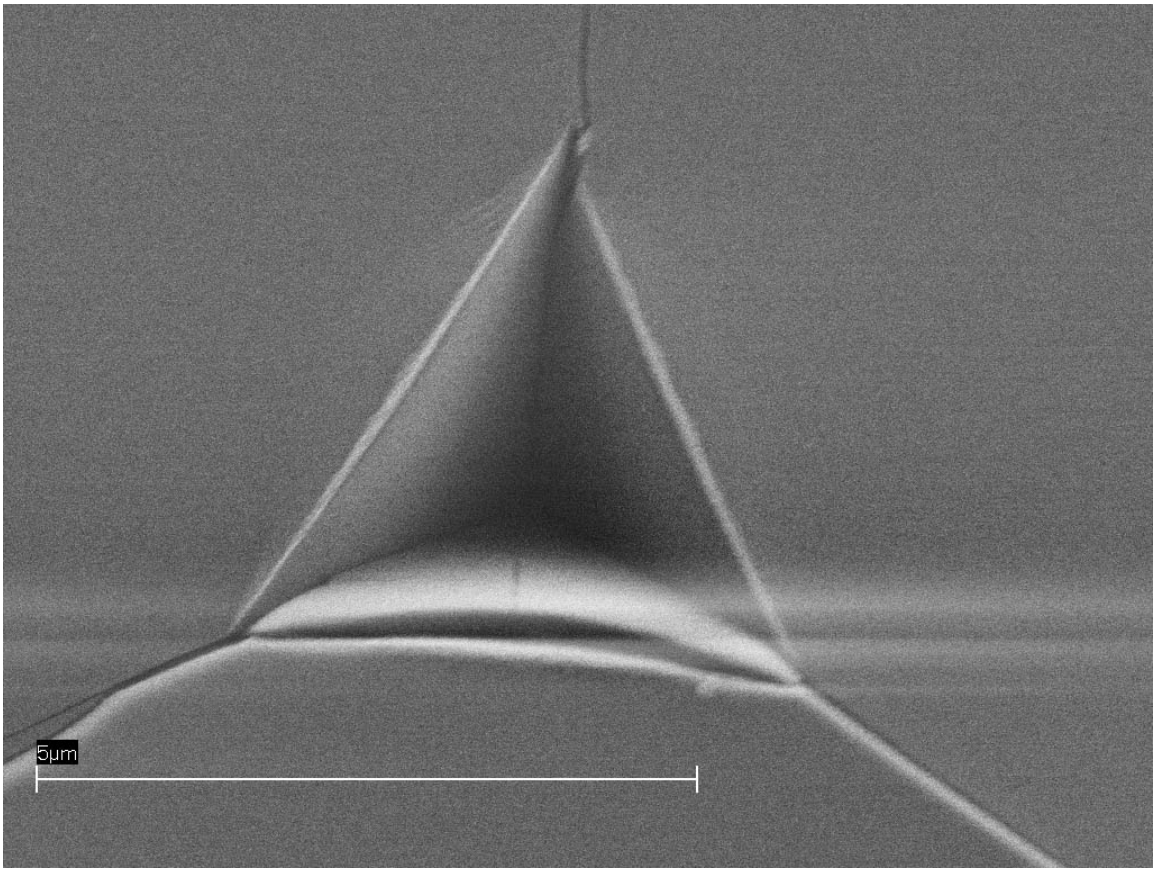

Figure 50 SEM image of 35.3^{o} indent

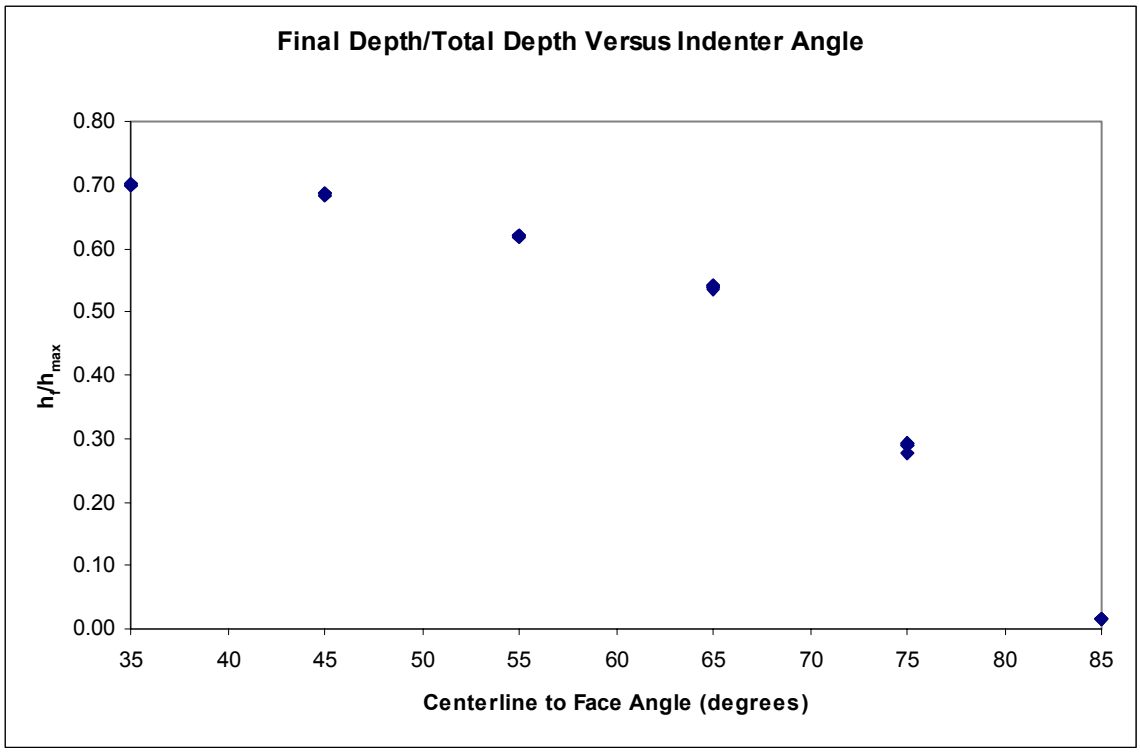

Figure 51 h_f/h_{max} versus indenter angle

depth)/h_{max}(maximum depth) versus indenter angle. This clearly shows that the 85° indenter is almost completely elastic and fully developed plasticity only really occurring in the 45° and 35° indents. The rest of the indents lie in a transition region where elasticity plays an increasingly important role as the indenter angle increases.

3.6 Comparison of Measured β to Literature

Several attempts have been made in the past to determine what value of β should be used in indentation. Originally, the stiffness equation was derived for a rigid axisymmetric punch of arbitrary smooth profile in a linearly elastic medium where the small strain assumption applies [2]. For these limited cases, β is exactly one. Real pyramidal indenters deviate from axisymmetry creating stress singularities at their edges and deviate markedly from ψ=90°, which invalidates the small strain assumption. The most commonly used correction was presented by King [4], who used numerical methods to find $\beta = 1.034$ for a triangular flat ended punch in an elastic half space. Vlassak and Nix later conducted independent numerical calculations for the flat-ended triangular punch in an elastic medium using a more precise method and found a higher value, β = 1.058 [11]. Since real indentations occur in elastic-plastic materials, the pressure distribution of a flat punch in an elastic half-space should be altered by material yielding near stress singularities. Using this rationale, Hendrix conducted an elastic calculation using a flat pressure distribution for a triangular flat punch which yielded β = 1.023 [12]. Other studies have used finite element analyses to predict a value for β. Larson et al. conducted studies using a true 3D Berkovich pyramid in elastic and four different elastic-

plastic materials that simulate various aluminum alloys. Their simulations indicated that the value provided by King of β = 1.034 was preferable for elastic-plastic indentation [13] and yielded errors of less than 6.5% in the contact area. More recent studies by Hay et al. using analytical and FEA for a 2D elastic half-space yielded the following equation for indenters with a large included half angle [14]:

$$\beta = \pi \frac{\pi/4 + 0.15483073\cot(\psi)\frac{(1-2\nu)}{4(1-\nu)}}{\left(\pi/2 - 0.83119312\cot(\psi)\frac{(1-2\nu)}{4(1-\nu)}\right)^2}, \qquad 21$$

and for sharper indenters like the cube-corner:

$$\beta = 1 + \frac{(1-2\nu)}{4(1-\nu)\tan\psi}. \qquad 22$$

These relations suggest that β should increase with decreasing ν and ψ, as is the case with sharper indenters of this study. Finite element studies by Cheng and Cheng using a 68° cone in an elastic-perfectly plastic medium found that β = 1.05 independent of E/σ_y [15], and a second study for elastic-work hardening and elastic-perfectly plastic materials found β = 1.085 independent of E/σ_y and the work hardening coefficient n [16]. A recent review by Oliver et al. [6] suggests that for real indentations, we should disregard strictly elastic simulations as they do not consider the formation of the hardness impression. Using this rationale they suggest, β for the Berkovich indenter should fall in the range $1.0226 < \beta < 1.085$ with the most compelling choice being $\beta = 1.05$ which falls remarkably close to the value calculated in this study of $\beta = 1.055 \pm 0.021$ for the Berkovich indenter.

As noted by Martin and Troyon, when using β to determine area functions, the value of ε a correction factor in the equation

$$h_c = h_{\max} - \varepsilon \frac{P_{\max}}{S} \qquad 23$$

becomes an important quantity to monitor as even if the correct value of β is known, an error in this quantity can distort a calculated area function. They determine the value of ε to be:

$$\varepsilon = m\left\{1 - \frac{m-1}{m\left[\chi\left(\frac{m}{m-1}\right)\right]}\right\}, \qquad 24$$

where m is a fitting parameter in equation:

$$P = B\left(h - h_f\right)^m \qquad 25$$

that models the unloading curve. They report for a Berkovich indenter in fused quartz a value of $\beta = 1.063$ based on their determination of ε from careful load displacement data assuming an ideal conical indenter with a spherical tip They further point out that using the standard $\varepsilon = 0.75$ yields $\beta = 1.043$ [17]. Both of the values presented by Martin and Troyon fall within the error predictions of the value calculated in this study.

A comparison of the results of this work and other's attempts to characterize β as a function of indenter angle for a purely elastic medium are shown in Figure 52. In this figure, for all conical indentation cases, the value of centerline-to-face angle is the angle

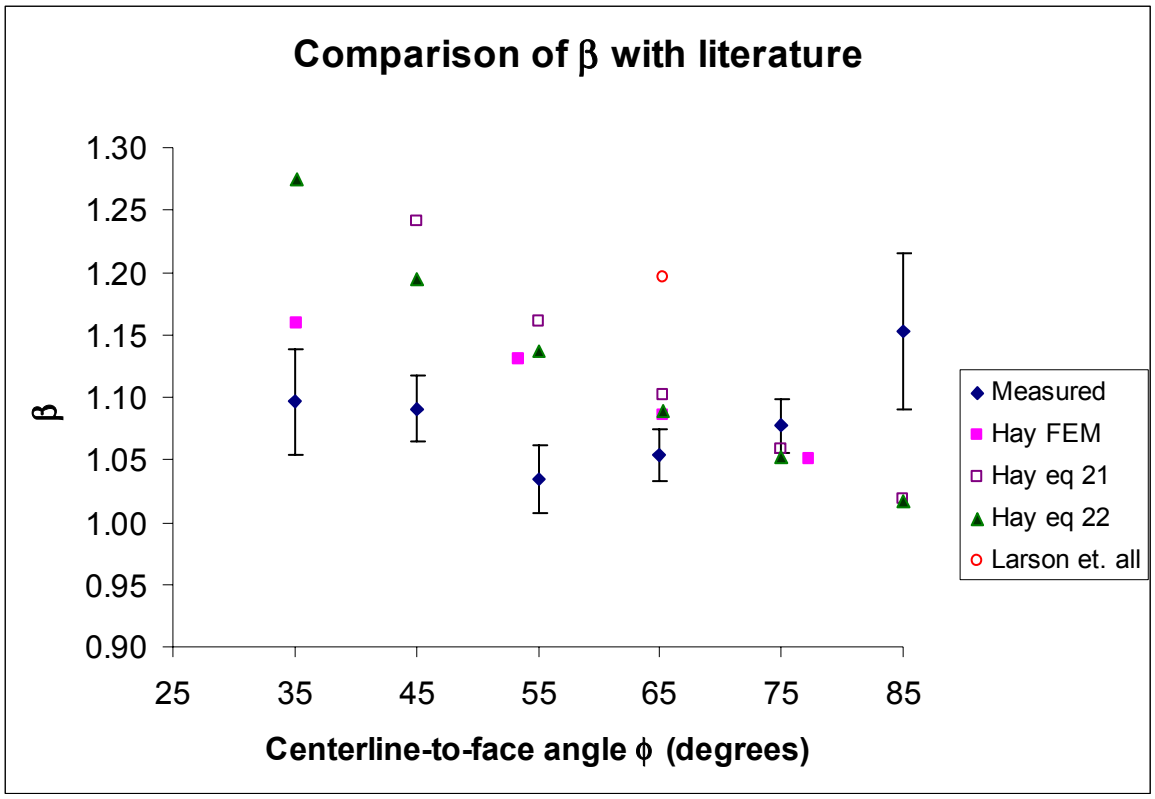

Figure 52 Measured β compared with literature (Error bars represent total error)

that gives the equivalent depth to area ratio. Hay et. al.'s [14] finite element solution for various cone angles ψ for a Poisson's ratio ν of 0, 0.2, and 0.4 have been linearly interpolated to $\nu = 0.13$ for comparison with results from this study in Figure 52.

The increasing trend of β as α decreases from 65^o falls in line with the predictions put forth in the work of Hay et al [14] as well as the FEA simulations in this study; however, the increasing trend as α grows larger than 65^o was completely unexpected and contrary to all the literature results as well as FEA calculations. One might expect the value of β for the wide angle indenters to tend toward the value presented in [4] of $\beta =$ 1.034 or Vlassak and Nix's more precise recalculation of the problem with a value of $\beta =$ 1.058 [5] which calculates β assuming a triangular flat punch in an elastic medium, as the shape of the indenter is approaching that of a triangular flat punch showing only elastic recovery. $\beta = 1.15$ for the 85^o indenter from this study seems to conflict markedly with this calculation. One possibility may be the pressure distributions. While the contact is nearly elastic, the pressure distribution between the indenter and the material is completely different. For simplicity, the pressure distributions for a 3D axi-symmetric cone and a circular punch will be compared. For a purely elastic case, the pressure distribution under a flat punch is of the form:

$$p = p_0 \left(1 - \frac{r^2}{a^2}\right)^{\frac{-1}{2}}, \qquad 26$$

which reaches a theoretically infinite value at the edges of the punch. On the other hand, the pressure distribution under the cone is given by:

$$\rho(r) = \frac{1}{2} E_r \cot(\alpha) \cosh^{-1}\left(\frac{a}{r}\right), \qquad 27$$

which decays to zero at the edges of contact. The pressure must decay for all indenters with smooth surfaces because if a finite pressure existed at the edge of the punch then the surface of the sample would show an infinite value for its slope at the edge of contact, where conical indenters have a fixed slope causing them to overlap [18]. Even as a conical indenter approaches $\alpha = 90^{o}$, its pressure distribution must be of the form in Eq. 27; therefore, it will be fundamentally different than a contact from a flat punch of similar size [17]. Also, as noted by Hendrix [12] the inherent plasticity in the material would tend to negate any stress singularities at the apex or near the edges, thus changing the pressure distribution away from the ideal pyramid. In addition to conducting 3D Berkovich elastic-plastic FEM experiments, Larsson et. al. [13] also conducted 3D Berkovich elastic simulations. In this case, they measured β to be

$$\beta = 1.2304\left(1 - 0.21\nu - 0.01\nu^2 - 0.41\nu^3\right), \qquad 28$$

which for the case of $\nu = 0.13$ as in our material Eq. 28 yields $\beta = 1.20$, which is remarkably close to our measured value of β for the 85° indenter of 1.21. Since the 85° indents are almost exclusively elastic, one might conclude that the value of β measured would fall in line with Larsson's result since it encompassed the true 3D nature of a 3-sided pyramidal indenter and only includes elasticity; however, this value is in conflict with the value calculated from the FEA analysis of $\beta = 1.09$ for the 85° elastic case. The

FEA also fails to suggest an increase in β with respect to indenter angle possibly pointing to potential errors as of yet unaccounted for in measuring β for very large indenter angles. The true reason for this discrepancy remains unknown. A value of β that is too large would suggest that the chosen contact area is too small, but in order to choose a contact area that brings the value of β in line with the literature requires many parts of the contact to lie within the region of partial contact where the gold is not adequately smoothed out. Evaluating Eq. 27 using the equivalent cone angle $\psi = 86.1^{o}$ ($\alpha = 85^{o}$) and a value of α that produces the same area as was measured in the 85^{o} case (a = 6.2μm) gives us a pressure of 0.6GPa 97% of the distance of the contact away from the center out of the contact, which is close to the bulk hardness strength for gold. A hardness value of 1GPa is a reasonable estimate of the hardness of heavily cold worked gold, and this corresponds to a point which is 92% of the radius of contact from the tip of the indenter. If the pressure needed to smooth out the cracks in the gold film is the same as the hardness, then this effect could possibly bring the value for the $\alpha = 85^{o}$ indenter down to $\beta = 1.15$, which is still well above theoretical predictions. This hardness of the gold coating may be even higher as it could be behaving as a layer of nanoparticles potentially lowering β even more. This pressure distribution is shown in Figure 53. The quandary of the increasing value of β for $\alpha = 85^{o}$ may require more study before it is resolved.

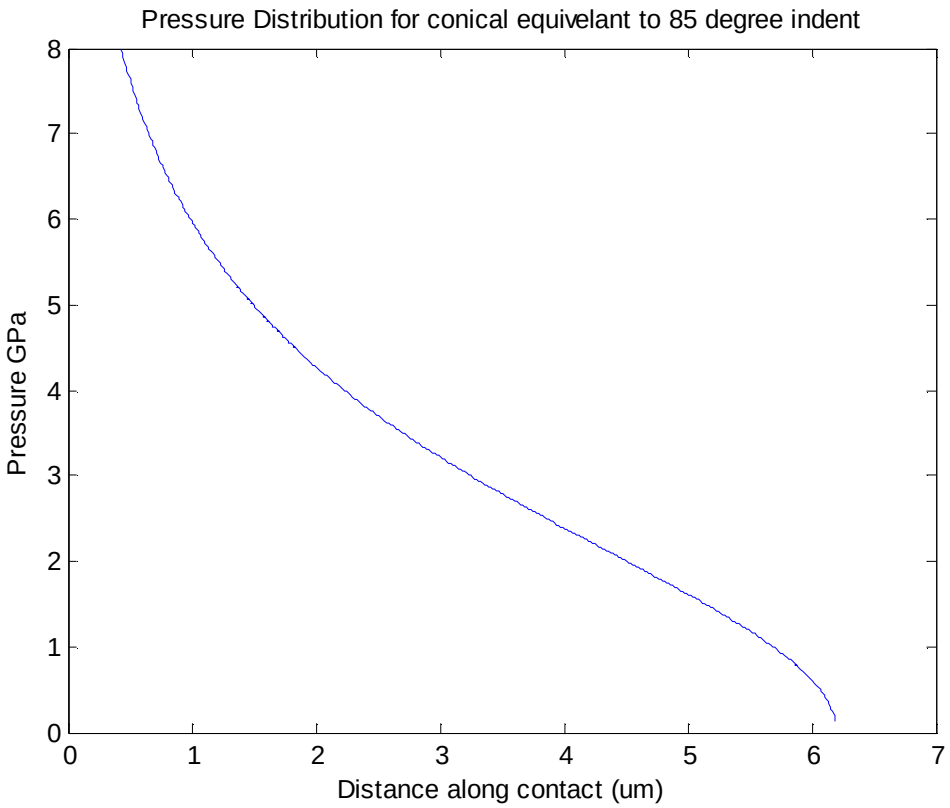

Figure 53 Pressure distribution for a cone approximately equivalent to an $\alpha = 85^{o}$ indent

4 Conclusions

(1) Based on careful measurements of contact area, contact stiffness, and elastic properties, the best estimate of the constant β for the Berkovich indentation of fused quartz is 1.055 ± 0.021.

(2) Other experimental measurements using triangular pyramidal indenters show that β is a function of indenter angle, exhibiting a minimum in the range α = 55°- 65°.

List of References

List of References

[1] W.C. Oliver and G. M. Pharr. *J. Mater. Res*. **7,** 1564 (1992).

[2] G.M. Pharr, W.C. Oliver, F.R. Brotzen, *J. Mater. Res.* **7**, 613 (1992).

[3] I. N. Sneddon, Int. J. Eng. Sci **3**, 47 (1965).

[4] R.B. King, *Int. J. Solids Structures* **23**, 1657 (1987).

[5] Hay, J. L. and Pharr, G. M., ASM Handbook Volume 8 (2000).

[6] W.C. Oliver and G.M. Pharr, *J. Mater. Res.* **19**, 1 (2004).

[7] H. Bei, E.P. George, and G.M. Pharr, *Scripta Mater.* **51,** 875 (2004).

[8] Shim, Sanghoon, Email Correspondence, March (2005)

[9] Taylor, John R. *An Introduction to Error Analysis. Second Edition.* Sausalito, CA: University Science Books, 1997.

[10] Bei, H. Email, Correspondence, EC of FS September (2004)

[11] J.J. Vlassak and W.D. Nix, *J. Mech. Phys. Solids*, **42**, 1223 (1994)

[12] B. C. Hendrix, J. Mater. Res. **10**, 255 (1995).

[13] P-L. Larsson, A. E. Giannakopoulos, E. Soderlund, D.J. Rowcliffe, and R. Vestergaard, Int. J. Solids Structures **36**, 2 pg 221 (1996).

[14] Hay, Jack C Bolshakov, A. and Pharr, G. M., J. Mater. Res **14**, 6 pg 2296 (1999).

[15] Y-T. Cheng and C-M. Cheng, *Int. J. Solids Structures* **36**, 1231 (1999).

[16] Y-T. Cheng and C-M. Cheng, *J. Appl. Phys*. **84**, 1284 (1998).

[17] M. Martin and M. Troyon, *J. Mater.* Res. **17**, 2227 (2002).

[18] K. L. Johnson. *Contact Mechanics*. Cambridge, University of Cambridge, 2001.

Appendix

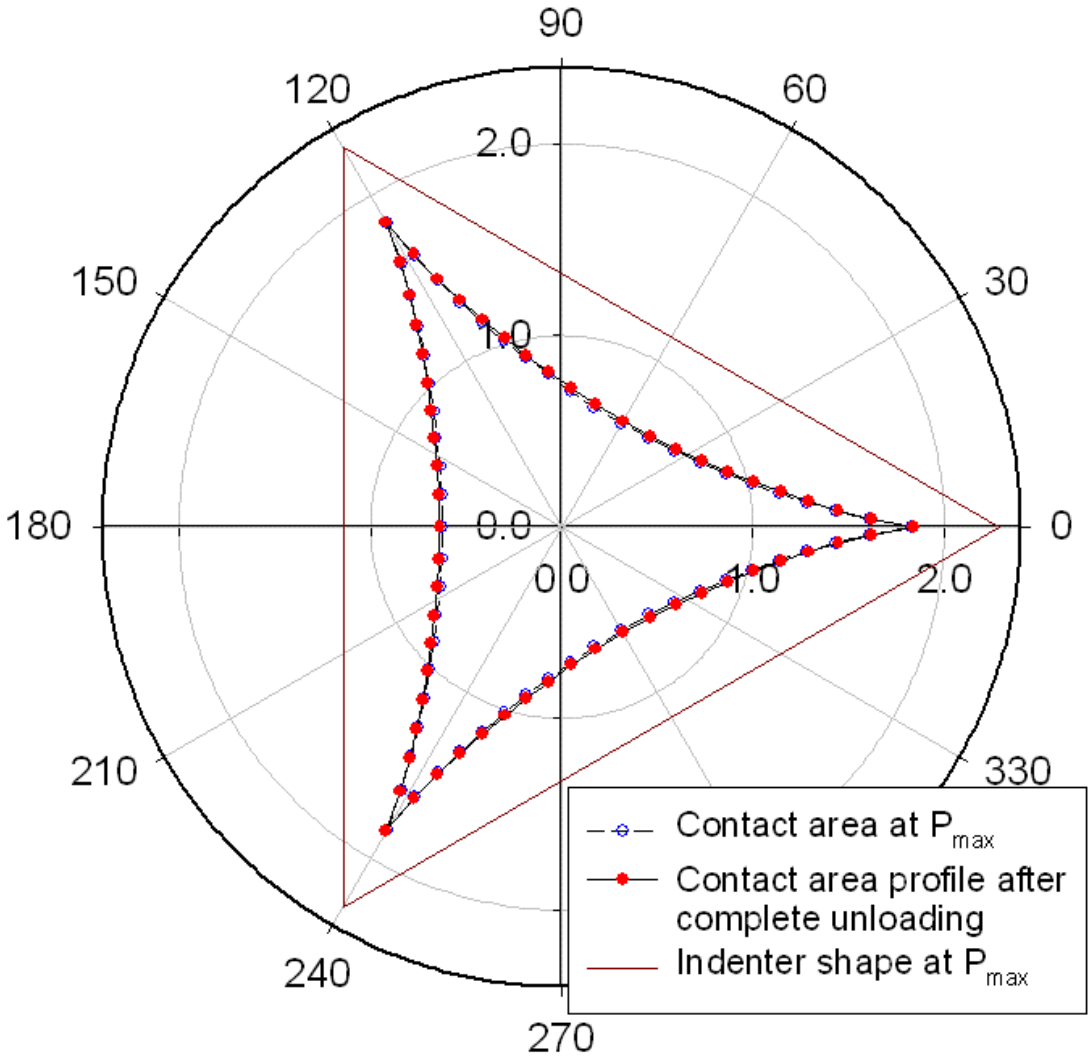

Figure A-1 3D FEA elastic recovery of 85^{o} frictionless indent

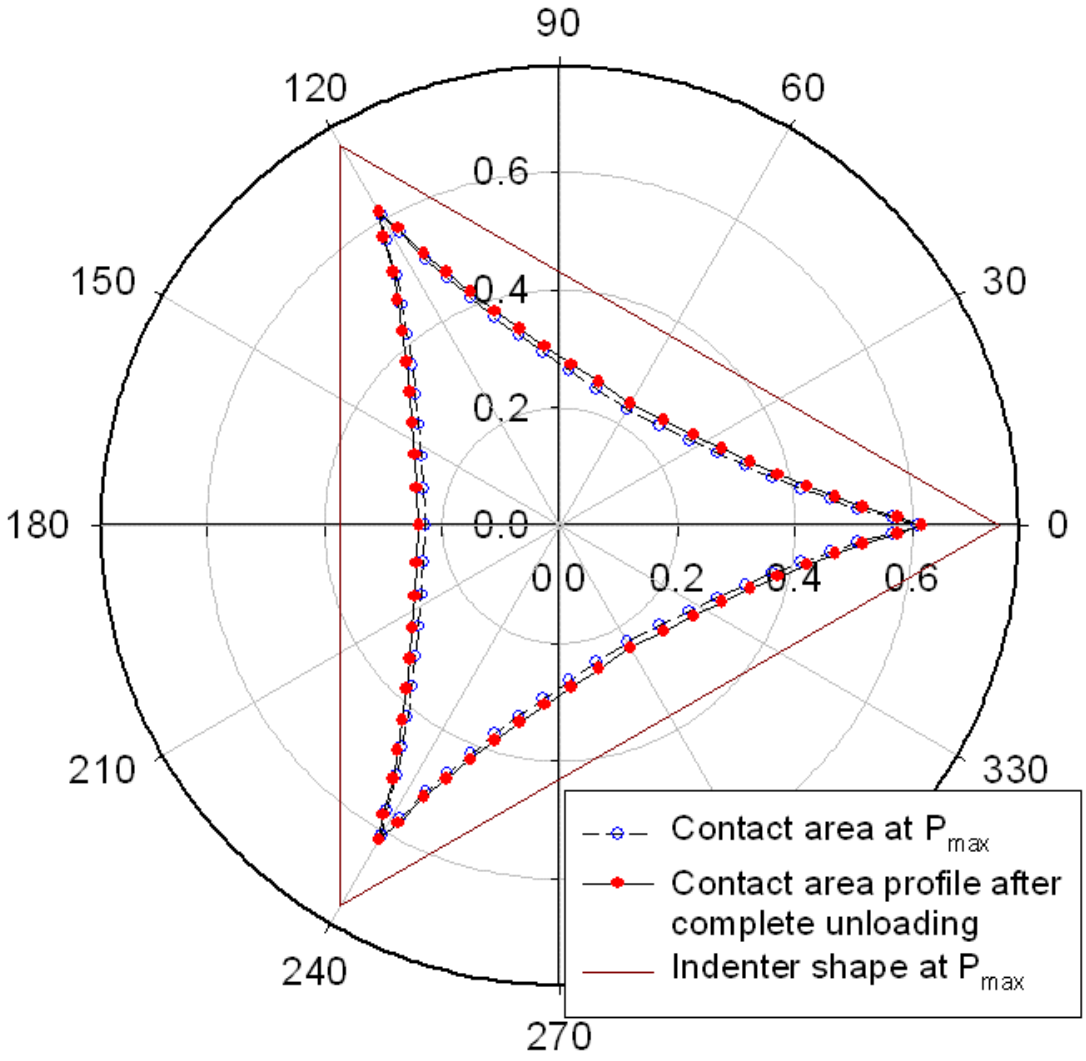

Figure A-2 FEA elastic recovery of 75^{o} frictionless indent

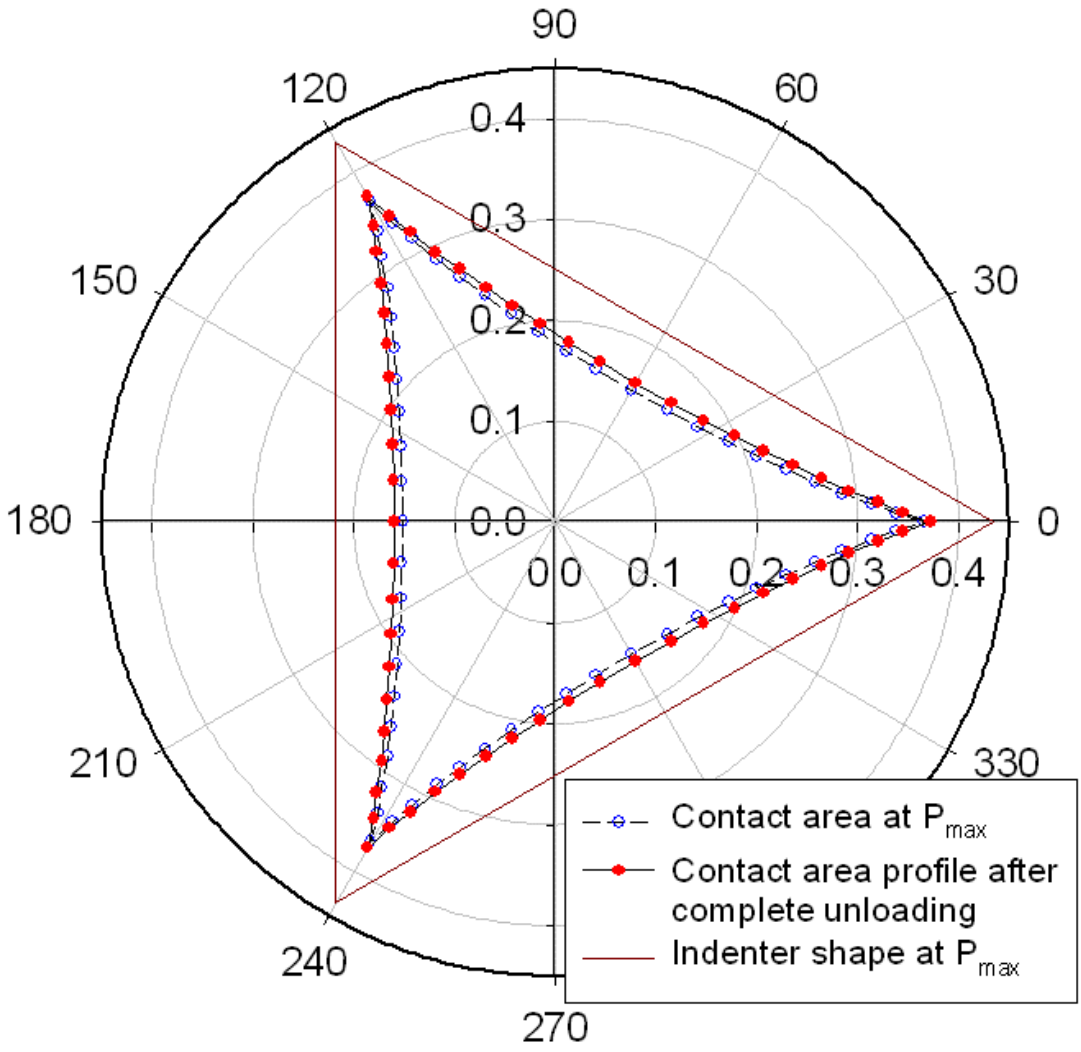

Figure A-3 Elastic recovery of Berkovich frictionless indent

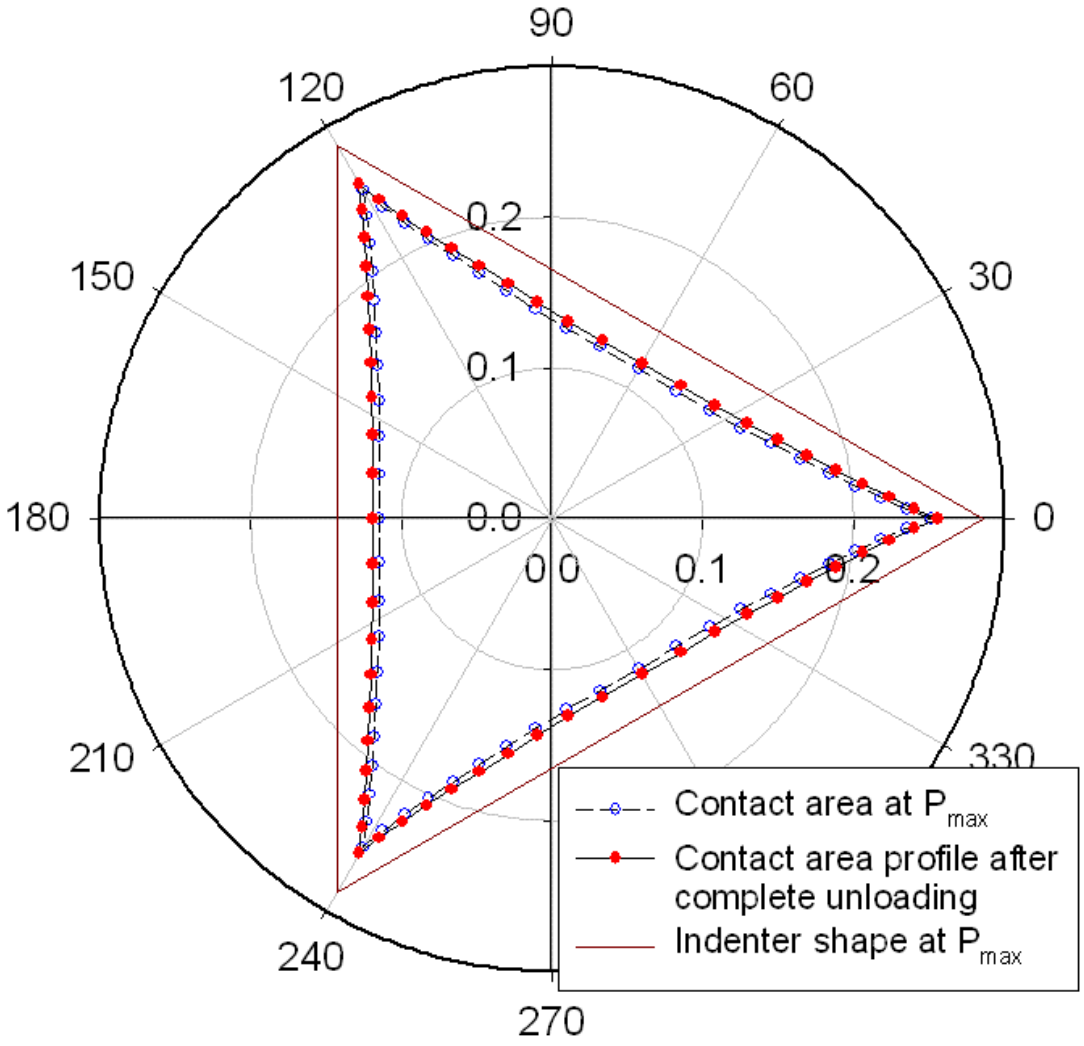

Figure A-4 FEA elastic recovery of 55° frictionless indent

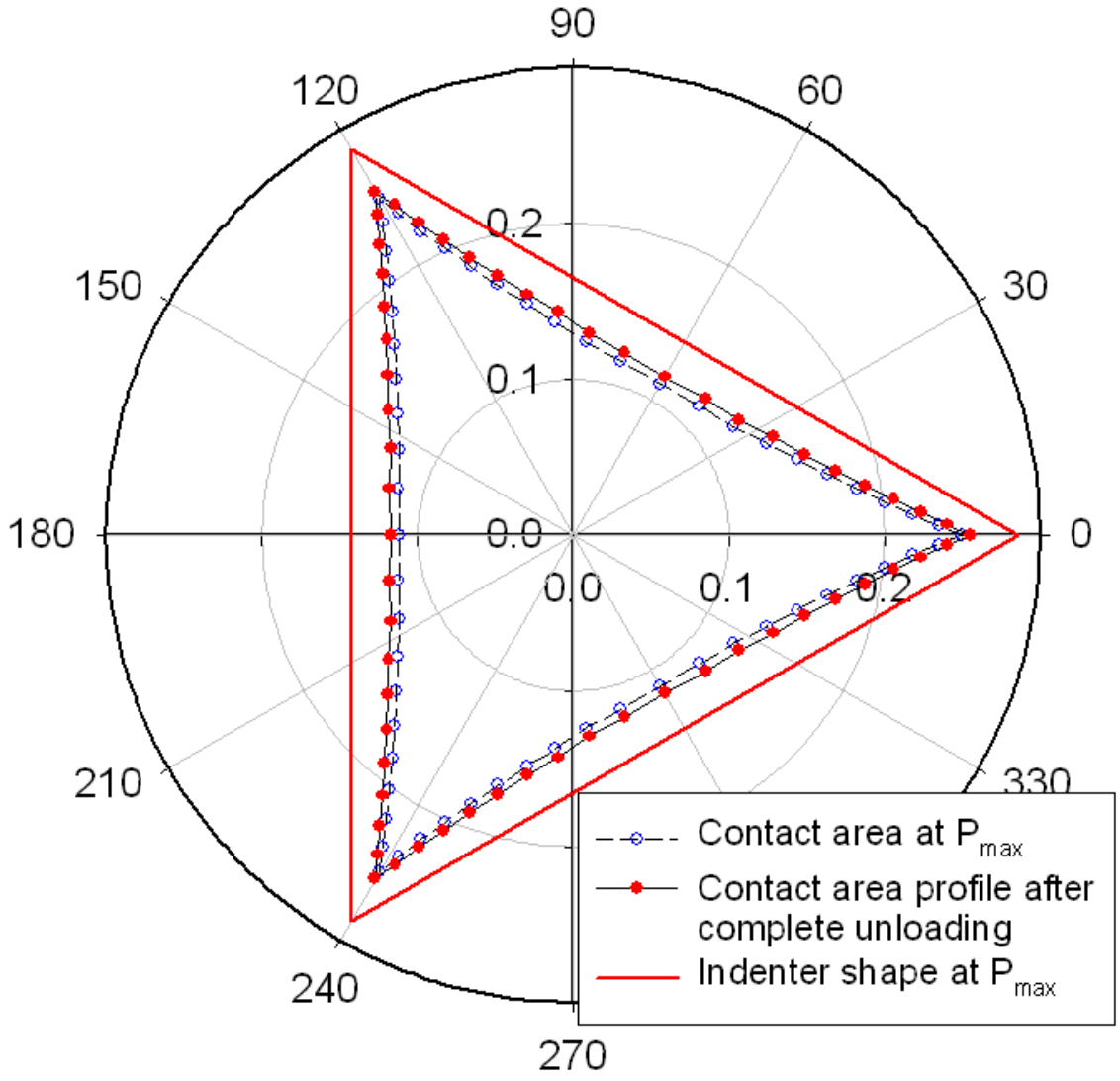

Figure A-5 Elastic recovery of 55^{o} indent μ=0.2

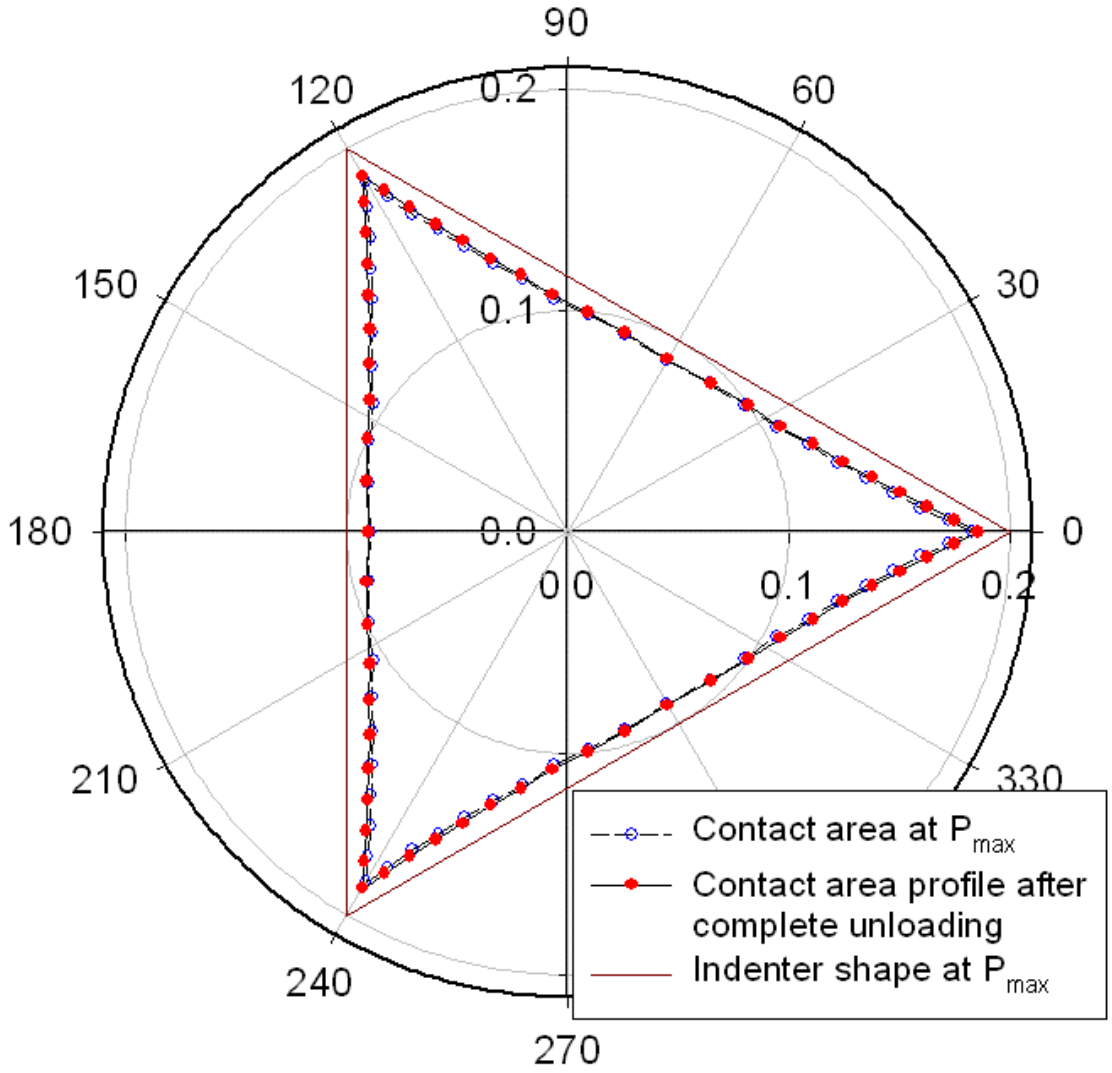

Figure A-6 FEA elastic recovery of 45^{o} frictionless indent

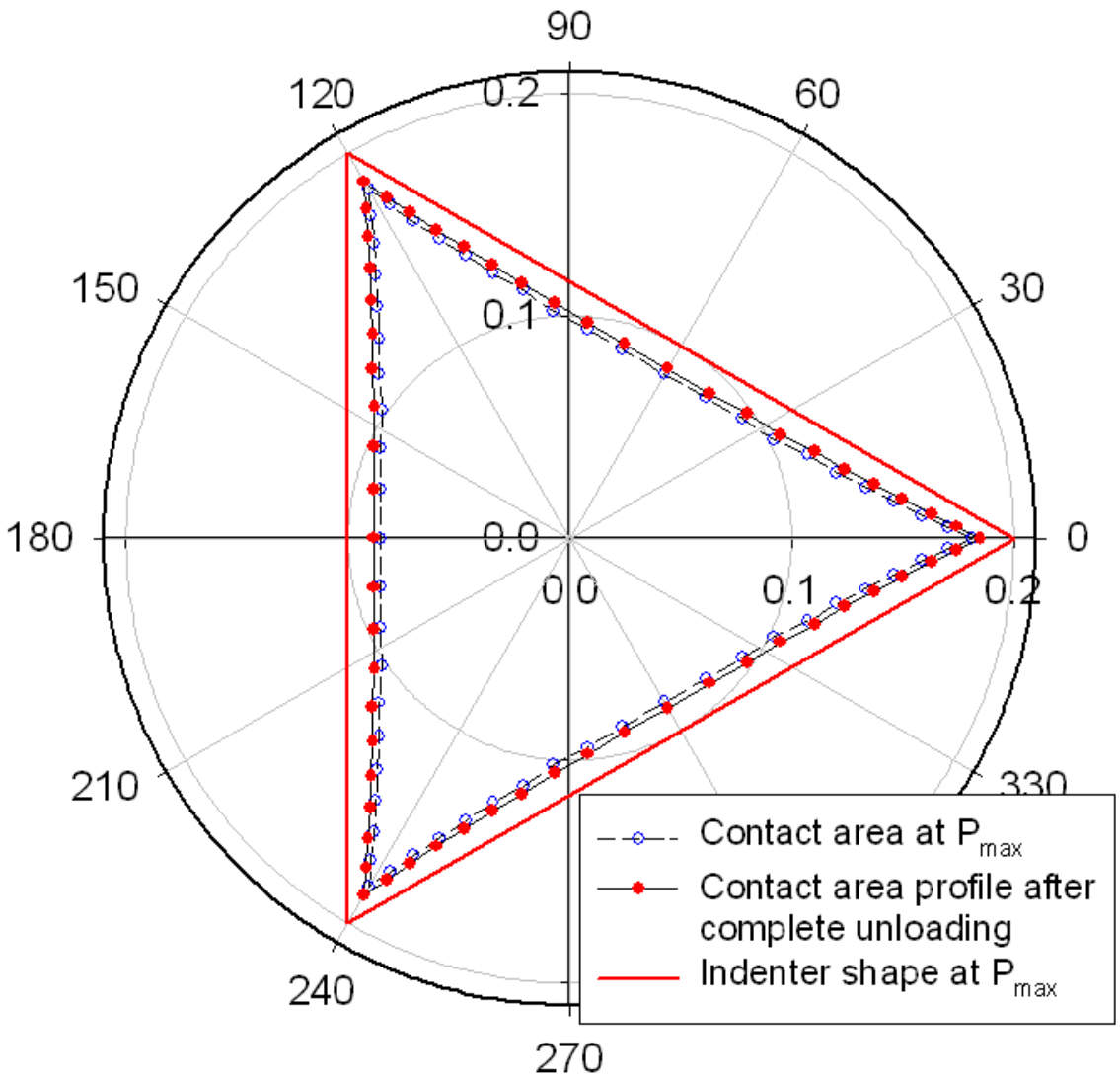

Figure A-7 Elastic recovery of 45^{o} indent μ=0.2

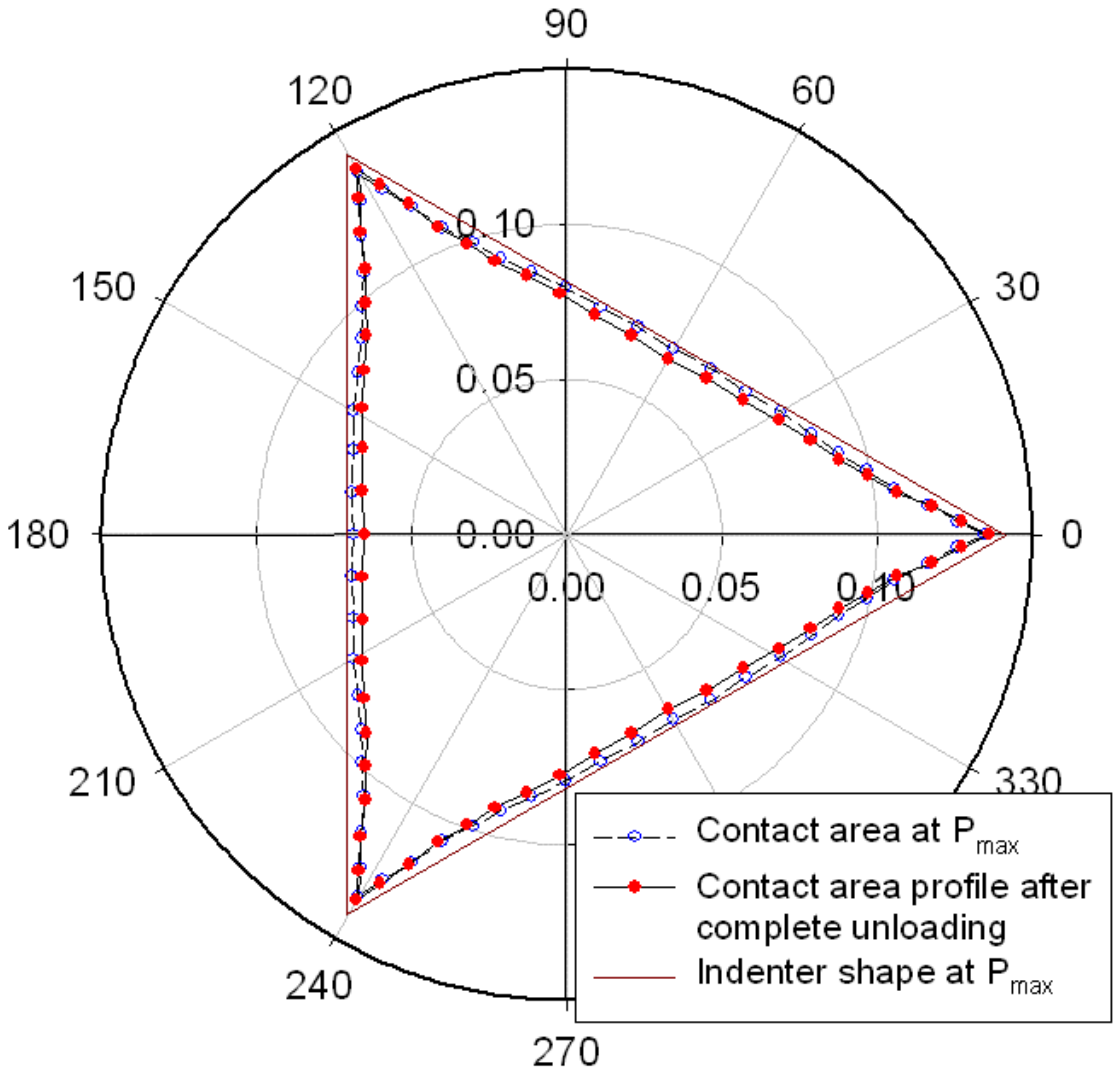

Figure A-8 FEA elastic recovery of Cube Corner frictionless indent

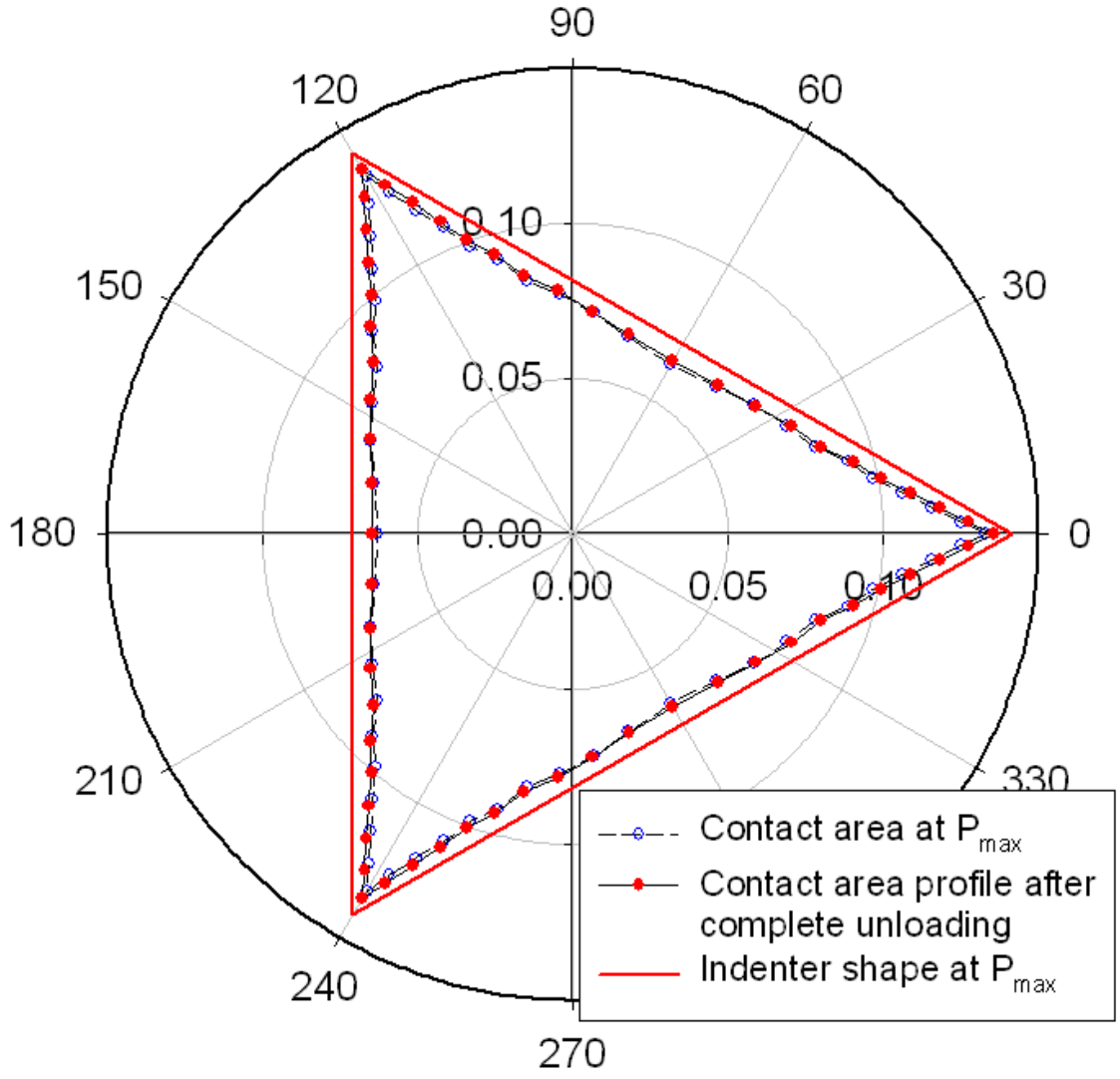

Figure A-9 Elastic recovery of cube corner indent μ=0.2

Vita

Jeremy Harper Strader was born in Knoxville, TN on June 22, 1977. He attended grade school in the Farragut school system in Farragut, TN. He graduated from Farragut High School in 1995. He then went to the University of Tennessee, Knoxville and then received a B.S. in Materials Science & Engineering in 2001.

Currently Jeremy is pursuing his Doctorate at the University of Tennessee in Materials Science & Engineering.